View metadata, citation and similar papers at core.ac.uk

brought to you by CORE

provided by University of Bergen

The role of the intermediate compartment in membrane traffic during different stages of the cell cycle

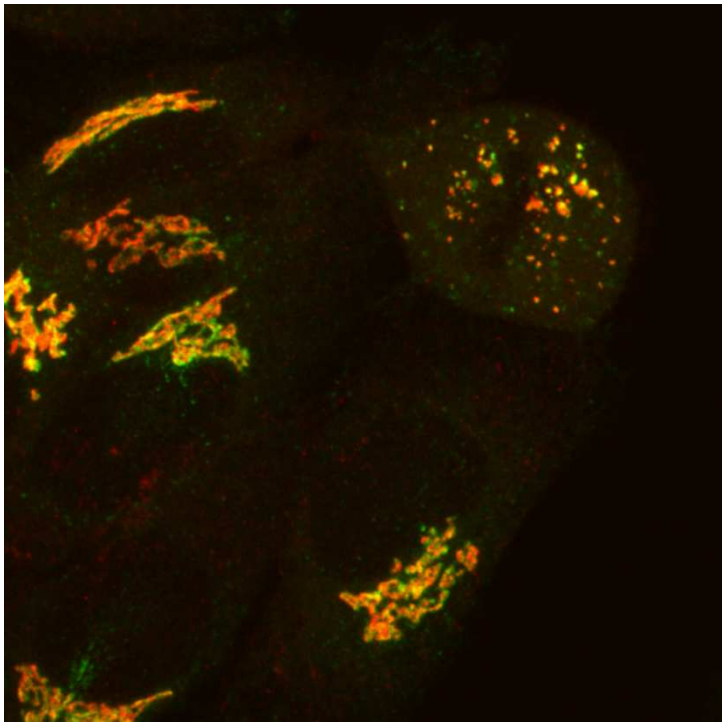

by

Nina Kouprina

A thesis submitted in partial fulfillment of the requirements
for a degree of Master of Science

Department of Biomedicine
Section of Anatomy and Cell Biology
Faculty of Medicine
University of Bergen
Norway

June 2011

Acknowledgments

This master thesis was carried out at the Department of Biomedicine, University of Bergen, Norway between September 2010 and June 2011 under the supervision of Professor Jaakko Saraste.

First and most of all, I would like to sincerely thank my supervisor, Dr. Jaakko Saraste. Through all the ups and downs, hopes and frustrations, and many successes and failures, you have always provided me with your guidance and encouragement every step of the way. I am very grateful to you for your help and support during the writing of this thesis, as well as for the many interesting and insightful discussions that we have had this year.

I am also very grateful to Dr. Michaël Marie for his assistance with confocal imaging, immunostaining, preparation of the figures, and most importantly, for his availability and willingness to help. An additional thanks to Endy Spriet for teaching me how to operate the confocal microscope.

Furthermore, I would like to thank Dr. Anni Vedeler and several people in her lab (Hanne Hollås and Aase Merethe Raddum) for their much-needed assistance with running gels when our system was not functioning. I would also like to thank Bodil Berger Hansen for her advice on SDS-PAGE and Western blotting.

Finally, I would like to thank my fellow master students for their friendship and support over the past two years.

Nina Kouprina

June 2011

Table of contents

Abbreviations

ADP/ATP Adenosine di/triphosphate

ARF1 ADP ribosylation factor 1

Baf A1 Bafilomycin A1

BFA Brefeldin A

CDK1 Cyclin-dependent kinase 1

CFTR Cystic fibrosis transmembrane conductance regulator

CGN *cis*-Golgi network

COPI Coat protein complex I

COPII Coat protein complex II

CQ Chloroquine

DAMP 3-(2,4-dinitroanilino)-3'-amino-*N*-methyldipropylamine

DAPI 4',6-diamidino-2-phenylindole

ER Endoplasmic reticulum

ERC Endocytic recycling compartment

ERES ER exit sites

ERGIC ER-to-Golgi intermediate compartment

FITC Fluorescein isothiocyanate

GBF1 Golgi-specific brefeldin A-resistance guanine nucleotide exchange factor 1

GDP/GTP Guanosine di/triphosphate

GEF Guanine nucleotide exchange factor

GFP Green fluorescent protein

GM130 Golgi matrix protein of 130 kDa

GRASP65 Golgi reassembly stacking protein of 65 kDa

HRP Horseradish peroxidase

IC Intermediate compartment

KDEL Lysine-aspartate-glutamine-leucine

KDEL-R KDEL receptor

Man II Mannosidase II

MEK1 MAPK/ERK kinase 1

MT Microtubule

NH_4Cl Ammonium chloride

NRK Normal rat kidney cell

pcIC Pericentrosomal intermediate compartment

PCMS Pericentrosomal membrane system

PLK1 Polo-like kinase 1

PM Plasma membrane

ROI Region of interest

SDS-PAGE Sodium dodecyl sulfate polyacrylamide gel electrophoresis

SNARE SNAP (soluble NSF attachment protein) receptor

SFV-G Semliki Forest virus glycoprotein

TGN *trans*-Golgi network

t-SNARE SNARE on target membrane

TxR Texas Red

V-ATPase Vacuolar-type H+-ATPase

v-SNARE SNARE on vesicle membrane

VSV-G Vesicular stomatitis virus glycoprotein

VTC Vesicular tubular cluster

Abstract

The biosynthetic-secretory pathway delivers newly synthesized molecules from the endoplasmic reticulum (ER) to the plasma membrane (PM), as well as to endomembrane compartments. The intermediate compartment (IC) is an interconnected membrane system, which mediates bidirectional trafficking at the ER-Golgi boundary. Besides operating in the classical secretory pathway, the IC also appears to participate in unconventional, Golgi-independent trafficking. Recent live-cell imaging studies have revealed that the IC is stably anchored next to the centrosome via its central domain, the pericentrosomal IC (pcIC). This novel structure, defined by the GTPase Rab1A, separates from the Golgi during cellular events involving centrosome relocation. This IC network also maintains its pericentrosomal positioning and dynamics after treatment with brefeldin A (BFA), a drug that results in the release of membrane-bound COPI coats and reversible Golgi disassembly. Thus, it was proposed that the pcIC acts as an important sorting site in both Golgi-dependent and -independent trafficking and therefore may be an acidic organelle. Based on the above findings, as well as recent results showing the persistence of the IC during mitosis, this study addressed the trafficking functions of this organelle throughout the cell cycle, with a special focus on its possible lumenal acidification.

Previous studies have provided evidence that the Golgi enzyme mannosidase II (Man II) continuously cycles between the IC and the Golgi apparatus. Treatment of interphasic cells with ammonium chloride (NH_4Cl) resulted in a delay in BFA-induced redistribution of Man II to the ER, leading to its temporary arrest in the pcIC, thus indicating that IC acidification plays a role in retrograde trafficking. By contrast, exposure of mitotic cells to NH_4Cl effectively blocked Man II redistribution into the Golgi haze, resulting in its accumulation in large Rab1A-containing membrane clusters at metaphase. Importantly, other acidification inhibitors (chloroquine and bafilomycin A1), as well as BFA, gave similar effects, supporting the conclusion that the IC is an acidic organelle. Moreover, as the IC maintains its BFA-resistant character during cell division, these results raise the interesting possibility that mitotic IC clusters operate as way stations during the redistribution of Golgi enzymes during mitosis. Accordingly, lumenal acidification appears to be required for the COPI vesicle-mediated dispersal of Golgi enzymes from the IC elements into the mitotic Golgi haze. Low temperature (15°C) was also observed to affect the mitotic redistribution of Man II; however, these preliminary results need to be verified by further experiments. Overall, the results in this thesis provide evidence that the sorting and trafficking functions of the acidic IC are regulated in a cell cycle-dependent manner.

1 Introduction

1.1 Overview of membrane traffic pathways

The complex system of endomembranes within the eukaryotic cell allows for the separation of biochemical reactions from the outside environment, as well as for the division of labor between different intracellular compartments [1]. In the 1960s and 1970s, many researchers, including the Nobel laureate George E. Palade, employed electron microscopy and cell fractionation to demonstrate that morphologically and compositionally distinct organelles perform different functions within a cell [1-3]. Subsequent studies on the interplay between these compartments led to the clarification of several common principles of intracellular trafficking. These principles will be briefly discussed below, as they are central to the topic of this thesis.

Transport between two compartments occurs via vesicular or tubular carriers that bud from a donor compartment and fuse with an acceptor compartment [1,2,4]. Because donor and acceptor compartments have biochemically unique membrane compositions, it is necessary to have mechanisms that preserve compartment identity during active communication [1]. One of these mechanisms is molecular sorting, which ensures that particular membrane components are either recruited to or excluded from the budding transport intermediates [1-3]. This is accomplished via interaction of forward-directed cargo with cytoplasmic adaptors and coats, and via processes that retain resident proteins within the donor organelle [1-3]. The second mechanism is vesicle targeting, which involves the delivery of transport intermediates to the appropriate acceptor compartment along cytoskeletal tracks, followed by specific membrane fusion [1-3]. Several transport machinery proteins, such as Rab GTPases, tethering factors, and SNAREs, operate in targeting by promoting compartment recognition and subsequent membrane fusion [1-3,5]. Membrane identity is also preserved by intercompartmental anterograde and retrograde pathways, of which the latter both recycles traffic machinery for reuse and retrieves resident proteins that have escaped from the donor compartment [1,2]. The principles of molecular sorting, vesicle targeting, and membrane recycling are illustrated in **Figure 1** below.

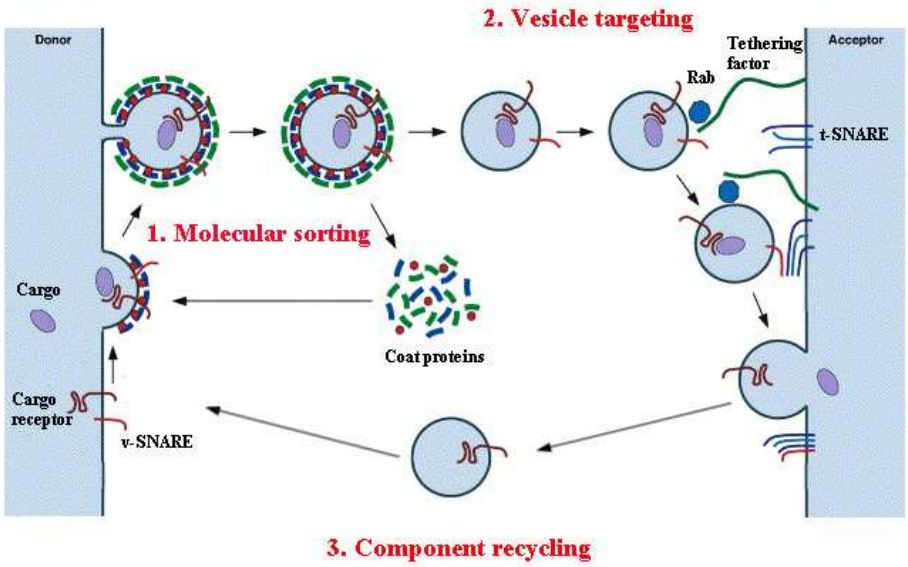

Figure 1. Principles of intercompartmental trafficking. The key steps of intracellular membrane traffic include molecular sorting (1), vesicle targeting (2), and the recycling of components (3). Molecular sorting involves the selective recruitment of forward-directed cargo into budding transport vesicles. This may be accomplished via cargo receptors, which in turn interact with coat components. Molecular sorting also results in the retention of resident proteins in the donor compartment (not shown). Vesicle targeting involves the directed delivery of transport intermediates to the appropriate acceptor compartment, followed by specific membrane fusion. This process is accomplished by proteins present on both vesicle and target membranes, including Rabs, tethering proteins, and SNAREs. Finally, component recycling involves the recovery of trafficking machinery (e.g., cargo receptors or SNAREs) for reuse, as well as the retrieval of escaped resident proteins to the donor compartment (not shown). Adapted from Reference [2].

1.1.1 Overview of the biosynthetic and endocytic pathways

The biosynthetic-secretory pathway (**Figure 2**) delivers newly synthesized lipids, proteins, and protein-bound carbohydrates from the endoplasmic reticulum (ER) to the plasma membrane (PM), as well as to endomembrane compartments, such as lysosomes [6,7]. This pathway is particularly pronounced in specialized secretory cells that release, for example, hormones or neurotransmitters into the extracellular space [6]. During the process of translation, peptide sequences signal protein translocation from the cytosol into the ER lumen, where proper folding and preliminary covalent modification occur [6]. Proteins are subsequently packaged into COPII-coated vesicles and move to the Golgi apparatus, where they undergo a series of post-translational modifications, such as glycosylation and phosphorylation, catalyzed by resident Golgi enzymes [6]. Upon reaching the most distal part of the Golgi, the *trans*-Golgi network (TGN), secretory

proteins are packaged and targeted to their ultimate destinations in the cell [6]. This anterograde transport is balanced by retrograde pathways that return lipids and specific proteins to previous compartments in order to maintain the homeostasis of each organelle [6].

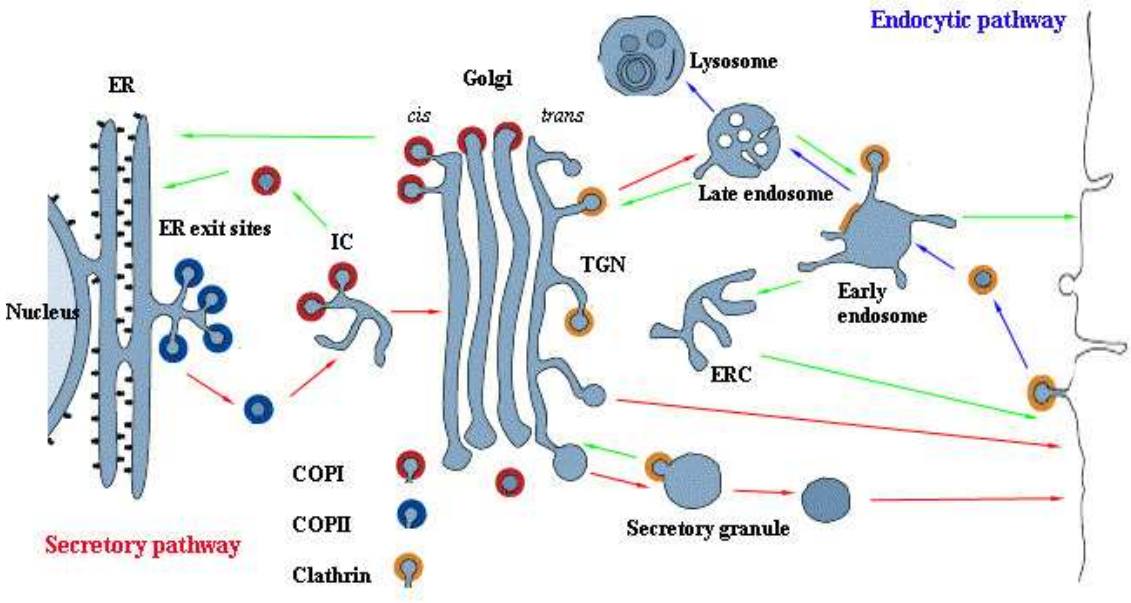

Figure 2. Simplified model of intracellular traffic routes. The biosynthetic-secretory pathway (red arrows) delivers newly synthesized cargo from the ER to the PM or the endosomal system, while the endocytic pathway (blue arrows) transports internalized molecules from the cell exterior to endosomes and lysosomes for degradation. Recycling pathways are shown in green. For simplicity, some recycling pathways are omitted. Refer to text for more details. ER, endoplasmic reticulum; IC, intermediate compartment; TGN, trans-Golgi network; ERC, endocytic recycling compartment; COP, coat protein. Adapted from Reference [2].

The endocytic pathway (**Figure 2**) delivers internalized molecules (e.g., nutrients, iron, cholesterol) from the PM to early endosomes and ultimately, lysosomes, where degradation can occur [6,8]. Specialized cells, such as macrophages, perform a special form of endocytosis called phagocytosis in order to ingest and subsequently degrade microorganisms or dead cells [6]. Endocytosis can occur via clathrin-coated pits found on the cytoplasmic surface of the PM or specialized cell surface invaginations called caveolae [6,8]. Vesicles derived from these regions of the PM selectively fuse with early endosomes, where internalized cargo and cargo receptors are sorted to different destinations in the cell [6,9]. Soluble cargo destined for degradation is released into the endosome lumen and transported to lysosomes via late endosomes, while cargo receptors are recycled back to the cell surface for reuse [6,9]. Multiple recycling pathways exist from the endosomal system back to the PM, as well as to the TGN [6,8,10].

1.2 Compartments of the early secretory pathway

1.2.1 Endoplasmic reticulum (ER)

Since protein synthesis occurs in the cytosol, secretory and membrane proteins must contain signal sequences that direct their translocation across the ER membrane [1]. Once inside the ER lumen, proteins are folded with the help of ER chaperones [6]. Proper folding produces proteins that are competent for transport, whereas unfolded or misfolded proteins remain bound to resident proteins in the ER and do not exit from this compartment [1]. Transport-competent proteins are packaged into COPII-coated vesicles located in ribosome-free regions of the ER called ER exit sites (ERES) [6,11].

There are two models of protein export from the ER. According to the bulk flow model, forward-directed cargo moves by default and does not require export signals [4,12,13]. By contrast, the receptor-mediated export model states that cargo proteins contain specific signals for their concentration and selective recruitment into budding COPII vesicles [4,12,13]. In accordance with the latter model, membrane proteins have been shown to contain exit signals in their cytosolic domains that are recognized by components of the COPII coat, while soluble cargo proteins possess signals recognized by transmembrane cargo receptors, which in turn are recognized by the COPII machinery [2,6,11,14]. The wide variety of soluble secretory cargo implies the existence of multiple binding sites or a family of recognition proteins [2,14].

1.2.2 Intermediate compartment (IC)

After their budding, ER-derived transport vesicles shed their coats and fuse with pleiomorphic vesicular tubular clusters (VTCs), which constitute the intermediate compartment (IC) [6,11,15,16]. The IC is an interconnected membrane network that consists of peripheral elements located adjacent to ERES, as well as more centrally located structures [9,14,16]. The peripheral elements merge together to form transport complexes that move along microtubules (MTs) and fuse with the central IC elements, finally delivering forward-directed cargo to the *cis*-Golgi [6,14,16]. The prevailing view is that the IC is a transient structure formed by homotypic fusion of COPII-coated vesicles [4,11,12,15,17]. However, recent live-cell imaging results obtained with fluorescent IC markers

(ERGIC-53/p58, Rab1) have provided evidence that the IC clusters are stationary in character and represent the site of formation of mobile anterograde and retrograde carriers [7,17-19]. The components of the IC are discussed in Section 1.3.

A major role of the IC is to sort anterograde and retrograde traffic [11,12,15]. The IC clusters possess COPI coats at their rims, and COPI-coated vesicles containing ER resident proteins and cargo receptors bud from the IC membranes, retrieving escaped ER proteins and transport machinery back to the ER [6,14]. Soluble ER proteins contain a common tetrapeptide KDEL sequence recognized by KDEL receptors (KDEL-Rs), which interact with COPI coats (see Section 1.3) [1,10,18], whereas certain integral proteins of the ER membrane contain KKXX/RRXX retrieval signals, which interact with COPI components directly [1,11]. Multiple rounds of COPI-mediated retrieval results in the concentration of secretory cargo within the IC elements [4,13,14,20]. However, it is also possible that besides retrograde trafficking, COPI-coated vesicles also function in the anterograde transport of proteins to the *cis*-Golgi [13,18]. Thus, sorting into the anterograde pathway from the IC could be signal mediated rather than occurring by default (see Section 1.3.2) [13,18]. The IC has also been implicated in Golgi-independent trafficking pathways, further described in Section 1.2.4.

1.2.3 Golgi apparatus

In mammalian cells, the Golgi is organized into a series of laterally linked stacks, each consisting of four to six flattened, membrane-limited cisternae located next to the nucleus and the centrosome [6,21]. Cargo moving through the Golgi apparatus enters the organelle at its *cis* face and undergoes a series of covalent modifications during its transfer across the cisternal stacks [6,21,22]. Accordingly, each cisterna is thought to contain a unique collection of processing enzymes, resulting in sequential processing of the cargo molecules [6,21]. The exact mechanism of intra-Golgi transport is still a matter of debate [6,10,22]. According to the vesicular transport model, cargo is transferred across stationary Golgi stacks via COPI-coated transport vesicles, which bud from one cisterna and fuse with the next [6,16,21,23]. There exists a parallel retrograde pathway also based on COPI vesicles, which retrieve resident Golgi proteins and return them to earlier compartments [6,23]. An alternative view, the cisternal maturation model, states that the cisternae progressively mature and migrate through the stack as new membrane is continuously added at the *cis* face of the Golgi and peeled off at its *trans* side [6,20,21,23]. Retrograde flow via COPI-coated vesicles

would be responsible for the maintenance of cisternal function by recycling enzymes back to the appropriate cisterna [6,20,23]. A further possibility is that cisternal progression and vesicle transport operate in parallel [20,23].

Regardless of the mechanism, proteins ultimately reach the TGN, where they are sorted and packaged into vesicles destined for various destinations [6,16,24]. Secretory traffic can reach the PM either via the constitutive pathway, also known as the default pathway, or via the regulated pathway (**see Figure 2**) [6]. Constitutive secretion does not require a particular signal and operates continuously [6]. By contrast, regulated secretion involves the sorting and storage of cargo in secretory vesicles or granules and its release via exocytosis in response to an extracellular signal (e.g., hormonal stimulation) [6]. There is also a third pathway involving molecules destined for lysosomes that operates by selective recognition in the TGN and subsequent delivery to lysosomes via endosomes (**see Figure 2**) [6].

1.2.4 Non-classical secretory pathways

In addition to the above described classical secretory pathway, there is evidence for pathways that bypass the Golgi apparatus [16,25]. In certain cases, this unconventional secretion is characterized by its insensitivity to brefeldin A (BFA) [25]. BFA is a fungal macrocyclic lactone that causes COPI dissociation from membranes leading to reversible Golgi disassembly and redistribution of Golgi enzymes to the ER [26,27]. The continued transport of some molecules (e.g., cholesterol, sphingomyelin, and certain proteins) to the cell surface in the presence of BFA implies either direct contact between the ER and PM or the existence of post-ER Golgi-independent pathways [25]. The latter possibility has been previously disregarded because BFA treatment was expected to disrupt IC structure [25]. However, recent experiments concerning IC morphology and dynamics have shown that this compartment is preserved as a dynamic network in drug-treated cells and thus can provide a direct link to the cell surface bypassing the Golgi [7].

Morphologically, the IC consists of compositionally distinct vacuolar and tubular domains [7,9,17,25,28,29]. The pleiomorphic vacuolar regions contain Golgi-bound cargo as well as the cargo receptor ERGIC-53/p58 (described in Section 1.3.1), whereas the tubules are defined by the GTPase Rab1A (described in Section 1.3.4) [7,9,28]. These tubules are highly dynamic and have been found to connect the peripheral and central IC elements, as well as establish a pathway from

the IC to the cell periphery [25,28]. This first described peripheral Golgi bypass pathway remains functional in BFA-treated cells, implying that it is COPI-independent and most likely dependent on Rab1 function (see **Figure 3** below) [9,25]. A similar pathway has been previously characterized in yeast [30].

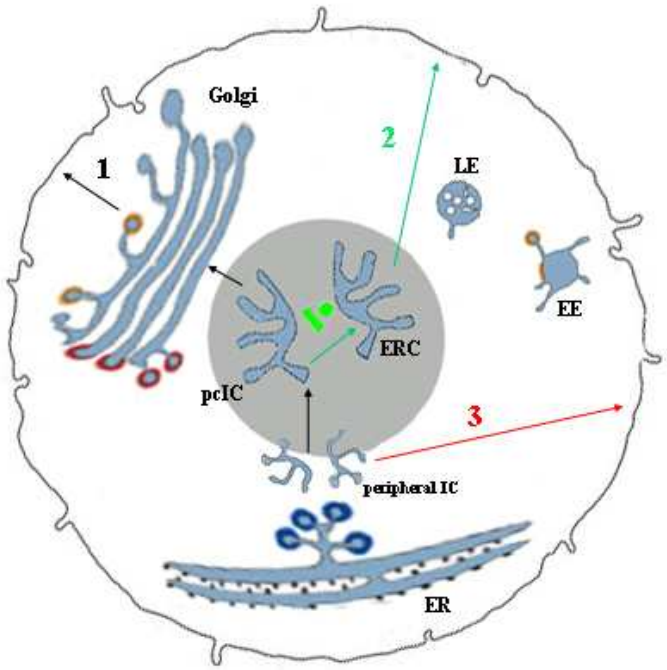

Figure 3. Role of the IC in biosynthetic-secretory trafficking. According to this model, the IC is involved in three major pathways to the cell surface. Secretory cargo from the ER moves to the pcIC, where trafficking diverges into two pathways: the classical pathway through the Golgi apparatus to the PM (1; black arrows) and a Golgi-independent pathway to the PM via the ERC (2; green arrows). There also exists a direct Golgi bypass route from the peripheral IC elements to the cell surface (3; red arrows). See text for more details. For simplicity, endocytic and recycling pathways are not indicated. The nucleus is shown in gray, and the centrosome in green. Note that this model depicts a cell in which the pcIC has separated from the Golgi. ER, endoplasmic reticulum; IC, intermediate compartment; pcIC, pericentrosomal IC; ERC, endocytic recycling compartment; EE, early endosome; LE, late endosome. Figure modified from Reference [31].

The visualization of IC dynamics in living cells via a fluorescent GFP-Rab1A construct resulted in the identification of a novel domain of the IC located adjacent to the centrosome and consequently termed the pericentrosomal IC (pcIC) [7,28]. While usually masked by the Golgi ribbon, its separation from the Golgi made it possible to identify the pcIC as a distinct structure [7]. This separation is coupled to cellular events that involve centrosome motility or Golgi reorientation (e.g., cell division or migration) [7]. ER-derived secretory cargo was observed to move toward this distinct pcIC, which is in turn connected with the Golgi via tubules [7].

Furthermore, the pcIC maintains its position and dynamics during BFA treatment (experimental Golgi disassembly) and thus was proposed to function as a way station in Golgi-independent trafficking (**Figure 3**) [7].

The endocytic recycling compartment (ERC) is another organelle located next to the centrosome [7,8,31]. There are several distinct recycling pathways from the ERC to the PM involving vesicular or tubular carriers [8,9]. These pathways mediate the recycling of internalized proteins and lipids back to the cell surface [8,9,31]. However, many newly synthesized proteins are also known to reach the PM via the ERC [31]. Interestingly, BFA treatment increases the overlap between the pcIC and ERC, which suggests the existence of a Golgi bypass pathway to the cell surface via the endosomal system (see **Figure 3**) [7,31]. Direct communication between the pcIC and the ERC can allow for non-conventional and in some cases, even BFA-resistant pathways to the PM bypassing the Golgi apparatus [7,9]. Importantly, the existence of a Golgi bypass pathway at the level of the pcIC suggests that protein sorting is initiated at a pre-Golgi location [9,31].

1.3 Components of the IC

1.3.1 ERGIC-53/p58

Human ERGIC-53 and its rat counterpart p58 are nonglycosylated type I integral membrane proteins [12]. ERGIC-53/p58 is highly concentrated in vesicular tubular IC clusters near the *cis*-Golgi and at the cell periphery, but is also present at lower concentrations in the transitional elements of the ER and the *cis* most cisterna of the Golgi [12]. It is particularly enriched in the vacuolar elements of the IC, but mostly absent from its tubular domain [31]. ERGIC-53/p58 functions as a cargo receptor during the transport of high mannose-containing glycoproteins from the ER to the IC [11,12]. A carbohydrate-recognition domain in its large lumenal portion is responsible for glycoprotein binding, whereas binding to the COPII coat involves an ER exit signal that includes a diphenylalanine motif located in the cytosolic domain of the protein [12]. In the IC, ERGIC-53/p58 releases its cargo and is recycled back to the ER via retrograde COPI-coated vesicles [12]. Correspondingly, it contains a KKXX ER targeting signal that binds to COPI components to mediate its recycling back to the ER [10,12]. ERGIC-53/p58 and other components of the IC are shown in **Figure 4**.

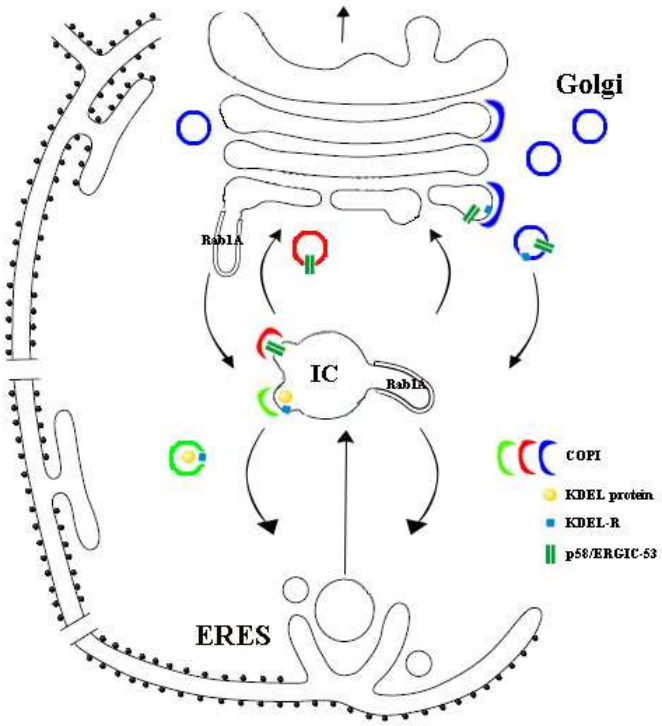

Figure 4. Components of the IC. The four best characterized components of the IC (or IC markers) are p58/ERGIC-53, COPI, KDEL-R, and Rab1 (only Rab1A isoform is shown). Note that according to this model, three different types of COPI coats are involved in anterograde and retrograde trafficking in the early biosynthetic pathway. COPI-independent, Rab1A-mediated tubular pathways are also depicted. See text for more details. ERES, endoplasmic reticulum exit sites; IC, intermediate compartment; COPI, coat protein I; KDEL-R, KDEL receptor. Figure modified from Reference [10].

1.3.2 COPI

COPI is a heptametric complex consisting of 4 large subunits (α, β, γ, δ-COP) and 3 additional subunits (β',ε, ζ-COP) [13,32]. The formation of COPI vesicles is regulated by the small GTPase ARF1, which is in turn activated by the guanine nucleotide exchange factor (GEF) GBF1 [10,13,32-34]. GBF1 first promotes ARF1 membrane insertion by stimulating GTP binding, and activated ARF1-GTP then recruits COPI to the membrane [13,32-34]. As mentioned in Section 1.2.2, the COPI system is involved in the retrograde transport of escaped ER resident proteins and cargo receptors from the IC and *cis*-Golgi to the ER (**see Figure 4**) [14,23,32]. Recent studies suggest that COPI also plays a role in the anterograde transport of cargo from the IC to the Golgi, indicating the existence of functionally distinct types of COPI vesicles (**see Figure 4**) [13,18,32]. Within the Golgi, COPI-mediated retrograde transport is thought to play a role in the generation of the polarized

distribution of Golgi resident proteins across the cisternal stacks [20]; however, the possibility that COPI vesicles participate in anterograde transport between Golgi cisternae cannot presently be excluded [23,32].

There are at least 3 biochemically distinct COPI coats in mammalian cells [7,22,35]. Two isotypes of both the γ- and ζ-COP subunits have been identified in higher eukaryotes, resulting in four possible combinations of the heptameric complex [32,35-37]. This finding may correlate with the existence of distinct COPI vesicle subpopulations that form in association with the peripheral and central IC elements or operate within the Golgi stacks [7,21,35]. Furthermore, the observed differential localization of the COPI subtypes suggests that the different coat complexes have distinct functions in the early secretory pathway [32,35]. This could explain the involvement of different COPI coats in both anterograde and retrograde traffic within the IC, as well as the findings showing that COPI vesicles can contain both anterograde and retrograde marker proteins [4,13,18,20,22,32].

1.3.3 KDEL-R

KDEL-R is a seven-pass transmembrane protein introduced in Section 1.2.2 [32]. As mentioned earlier, it is involved in the retrieval of escaped soluble ER resident proteins, which typically contain a KDEL sequence at their C-terminal ends [6,18]. Ligand binding to the receptor stimulates its oligomerization, which is followed by its interaction with COPI components via cytosolic KKXX signals [32]. KDEL-R rapidly cycles between the ER and Golgi, binding ER resident proteins in the IC and Golgi and returning them to the ER, where they are released from the receptor (**see Figure 4**) [6,16].

1.3.4 Rab1

Rab proteins are monomeric GTPases that play general roles in vesicle budding, targeting, and fusion [6,29,38]. Because these proteins specifically associate with the membranes of different organelles, they can function as molecular markers to define organelle identity and thus guide traffic between them [6,29,38,39]. Rab proteins cycle between an inactive GDP-bound state and an active GTP-bound state, which facilitates their binding to membranes [6,38,39]. The activation of a Rab protein from a GDP-bound state to the active GTP-bound state is accomplished by

membrane-bound Rab GEFs [6,38]. In their active state, Rab proteins can bind to various effectors, which play a wide range of roles in guiding coat assembly, vesicle transport, tethering, and fusion [5,6,38]. Thus, they are frequently considered as master regulators of membrane traffic.

Rab1 is localized to the ER-Golgi boundary, being specifically enriched in the IC membranes [6]. The two major effectors of Rab1, p115 and GM130, are both tethering factors that appear to regulate the fusion of ER-derived vesicles with the IC elements, as well as the transformation of the latter to *cis*-Golgi structures [5,7,18,39-41]. Rab1 is activated by a GEF close to the ERES and has been suggested to recruit p115 to the forming COPII vesicles [18,39,42]. Subsequently, p115 recruits a set of SNAREs that are required for fusion at the IC, acting as a catalyst for SNARE complex formation and membrane fusion [5,18,39,41,43]. In the Golgi region, p115 mediates membrane tethering via its interaction with GM130 [5,18,39,41-43]. This initial membrane docking is followed by SNARE-mediated fusion, which is also catalyzed by p115 [5,18,39,41]. Thus, by regulating the binding of p115 and GM130, Rab1 is thought to regulate the assembly of a SNARE complex and subsequent vesicle fusion events at the IC and *cis*-Golgi [5,39].

There are two Rab1 isoforms, Rab1A and Rab1B, which are both recruited to the IC membranes [7,29]. Both isoforms have been suggested to regulate anterograde transport between the ER and Golgi, as described; however, both are also found in tubular IC elements devoid of anterograde cargo, suggesting that they also function in retrograde transport to the ER [28]. The Rab1A isoform is preferentially recruited to the tubular domain of the IC (see **Figure 4**), whereas the Rab1B isoform appears to be associated with its vacuolar part [7]. As previously mentioned, Rab1A defines the pcIC and can be used to demonstrate its persistence after BFA treatment [7].

1.4 Role of acidification in the secretory pathway

1.4.1 Mechanisms of organelle acidification

The compartmentalization of eukaryotic cells allows them to create unique lumenal microenvironments and thus localize various biochemical reactions to specific intracellular compartments [44,45]. The catalytic activity of enzymes within these organelles is influenced by the intralumenal pH, which is optimal for the processing events that occur within a particular organelle [44,45]. Organelle acidification provides a mechanism to regulate optimal function of

many intracellular compartments, including endosomes, lysosomes, secretory granules, and the TGN [44,45]. Acidification is also required for the efficient sorting and trafficking of molecules along the endocytic and biosynthetic pathways [45]. Disruption of organelle acidification has been linked to complex diseases such as cancer, as well as genetic disorders such as Dent's disease and cystic fibrosis [45].

Steady state pH of an organelle is maintained by a balance between proton pumping to the lumen, proton leak, and counterion conductance [44,45]. Vacuolar H+-ATPases (V-ATPases) pump protons from the cytosol to the lumen of membrane-bound organelles harnessing the energy derived from ATP hydrolysis [44,46]. The variable density of pumps in different intracellular membranes, as well as modification of the activity of individual V-ATPase complexes, contribute to the observed pH differences of various organelles [46]. Moreover, proton pumping is counterbalanced by the intrinsic proton leak of a particular compartment membrane [44,46]. Differences in counterion permeability (e.g., chloride) additionally influence the extent of proton accumulation by affecting the membrane potential of a compartment [44,46]. Finally, second messengers may also play a role in pH regulation, and as a result, organelle pH may be influenced by the physiological state of the cell [46].

1.4.2 pH of the secretory pathway

The measurement of pH within organelles of the secretory pathway has been difficult because the compartments are not easily accessible to external pH-sensitive probes that are internalized by endocytosis [46]. Several techniques have been employed, including DAMP labeling and expression of pH-sensitive variants of GFP (such as pHluorin), which contain organelle-specific targeting sequences [45,46]. The ER is generally assumed to be neutral, having an approximate pH of 7.2 similar to the pH of the cytosol [46]. Subsequent compartments of the secretory pathway are thought to be more acidic, with the pH gradually decreasing from 6.7 in the *cis*-Golgi to 6.0 in the TGN [46]. Acidification of the TGN is important for protein sorting, as well as for the formation of secretory granules [44,45]. Notably, however, only the TGN and secretory granules have been convincingly demonstrated to be acidic compartments [45].

Whether low pH contributes to the function of earlier secretory compartments is less clear. Acidification has been shown to be important for the steady state localization of Golgi resident

proteins (e.g., glycosyltransferases) [47,48]. It also seems to play a role in retrograde trafficking in the early secretory pathway. pH neutralization by the V-ATPase inhibitor bafilomycin A1 was shown to selectively disrupt BFA-induced retrograde transport of the Golgi enzyme mannosidase II, resulting in its arrest in IC structures [45,49]. In addition, the IC has been found to contain an active V-ATPase [50], and DAMP staining has revealed that at least some of the centrally located IC elements are indeed acidic [45,49]. These results provide evidence for IC acidification and its role in retrograde trafficking [49]. The identification of the pcIC and its emerging role in protein sorting raise the question of its lumenal pH. Indeed, recent studies have shown that acidification inhibitors block the BFA-induced redistribution of Golgi components at the level of the pcIC, indicating that low pH is important for the function of this compartment in protein sorting [7].

1.4.3 Possible role of low pH in function of the IC

Although the current evidence for IC acidification is inconclusive, it is an attractive possibility, especially considering the multiple roles of this compartment in molecular sorting. A possible interplay between sorting and IC acidification is exemplified by the cycling of KDEL-R [6]. In order to be able to bind escaped soluble ER resident proteins in the IC and *cis*-Golgi and to release them in the ER, the affinities of the receptor for the KDEL sequence must differ in the two compartments [6]. Thus, in the IC and *cis*-Golgi, where ER residents are most likely found at low concentrations, the receptor must display a high affinity for the KDEL motif [3,6,32]. On the other hand, it must have a low affinity for the sequence in the ER in order to release its cargo [3,6,32]. Differential acidification of the early secretory compartments may play an important role in determining the affinity of KDEL-R for proteins containing the KDEL sequence [6,32]. In accordance with this idea, in vitro studies have shown that the binding of KDEL-R to the KDEL motif increases at lower pH [18,51].

In addition, differences in pH may be important for the dissociation of cargo proteins from recycling cargo receptors (e.g., ERGIC-53/p58) [18]. A lower pH in the IC may trigger the dissociation of cargo-receptor complexes, since neutralization of organelle pH has been shown to prevent the dissociation of ERGIC-53 and the cargo glycoprotein procathepsin Z [18,52]. Furthermore, the binding of ERGIC-53 to its glycoprotein cargo is calcium-dependent, and low calcium concentrations appear to increase the sensitivity of ERGIC-53 to pH [10,18]. Some studies have demonstrated high calcium levels in the Golgi and ER, but the lumenal calcium

concentration of the IC remains unknown [18,53]. One possibility is that low calcium levels and low pH together promote cargo release in the IC lumen [18,53].

1.4.4 Inhibitors of organelle acidification

Organelle acidification can be affected by various acidification inhibitors, such as weak bases, ionophores, and V-ATPase inhibitors [44]. Weak bases (e.g., chloroquine and ammonium chloride) are amine-containing membrane permeant compounds that disrupt organelle pH by accumulating in acidic compartments, where they become protonated and subsequently impermeant [45]. Proton ionophores, such as the Na^+/H^+ exchanger monensin, rapidly dissipate proton gradients in endocytic and biosynthetic compartments [45]. Finally, macrolide antibiotics, such as bafilomycin A1, dissipate the pH gradient by directly inhibiting V-ATPase activity [45,46].

The main problem with pH perturbants is that they cannot selectively disrupt the pH of individual compartments, and they most likely have indirect effects on other cellular processes [44]. For example, weak bases disrupt osmolarity and cause compartment swelling and vacuolarization [45]. In addition, because these treatments affect the pH of all acidified compartments, they may give rise to secondary effects [45]. For instance, disrupting the pH gradient in the TGN may also affect earlier steps in the secretory pathway [45]. Consequently, results from experiments utilizing these compounds should always be interpreted with caution.

1.5 Secretory pathway during mitosis

Successful cell division depends on duplication and equal partitioning of not only the genome, but also of intracellular organelles [40]. Because of the essential role of the Golgi apparatus in protein glycosylation, lipid biosynthesis, and secretory trafficking, its proper inheritance during mitosis is crucial for cellular homeostasis and function [40]. As a result, the mechanism of mammalian Golgi division is carefully coordinated with cell cycle progression [40].

According to the prevailing model, mitotic Golgi division involves several consecutive steps, which are briefly discussed below. During early prophase, the recruitment of COPII to ER membranes is blocked by a currently unknown mechanism, resulting in the inhibition of ER

export [54-57]. The Golgi ribbon is then laterally fragmented, and the cisternal stacks undergo further disassembly during prometaphase [40,56,58]. The resulting Golgi fragments (also known as mitotic Golgi clusters) are then transformed into a collection of vesicles and tubules during metaphase, resulting in the formation of a so-called mitotic Golgi haze [40,42,54,56,58-60]. In parallel with chromosome segregation, these mitotic Golgi clusters are equally partitioned between the forming daughter cells [40,56]. Mitotic Golgi disassembly is reversible, and the Golgi fragments again coalesce to reform two functional daughter Golgis at cytokinesis [40,56,59].

1.5.1 Mechanisms of mitotic Golgi disassembly

The mechanisms of lateral unlinking, cisternal unstacking, and further breakdown of the Golgi into vesicles and tubules depend on the phosphorylation of tethering factors such as GRASP65 and GM130 by the mitotic kinases CDK1/cyclin B, MEK1, and PLK1 [40,54,58,61]. GRASP65 is an important tethering factor that connects Golgi stacks laterally into a ribbon and links adjacent cisternae within a stack together via its ability to homo-oligomerize [5,39,40,56,62]. Phosphorylation of GRASP65 by CDK1 during late G2/early prophase disrupts oligomerization, resulting in disassembly of the Golgi ribbon and breakdown of connections between adjacent cisternae [5,39,40,42,56,62,63]. In turn, unstacking dramatically increases the area available for vesicle budding, possibly enhancing the COPI-dependent vesiculation process [39,40,56]. Consequently, by metaphase, the isolated stacks rapidly disperse into the mitotic Golgi clusters via increased formation of COPI vesicles [39,40,63]. Golgi fragmentation can also proceed in a COPI-independent manner, involving the transformation of cisternae into extensive tubular networks [4,33,40,64].

Golgi disassembly is also promoted by mitotic inhibition of vesicle tethering and fusion, mediated by CDK1-dependent phosphorylation of GM130 [5,39,40,43,54,56,61]. During interphase, GM130 is recruited to Golgi membranes via its association with GRASP65 and interacts with the cytosolic factor p115, which is bound to giantin on COPI vesicles [5,39-43,54,55,58]. This GM130-p115-giantin complex brings the two membranes together and catalyzes vesicle fusion [5,39-41,43]. During mitosis, GM130 phosphorylation interferes with the formation of this complex, leading to the inhibition of COPI vesicle docking and fusion, which in combination with increased vesicle budding and the inhibition of ER export, results in rapid fragmentation and dispersal of the Golgi during metaphase [5,39,40,42,43,54,56,58].

1.5.2 Golgi partitioning

There are two general models for mitotic Golgi partitioning, which differ in their definition of the nature of the mitotic Golgi haze [40,58,65]. According to one model, Golgi resident proteins are absorbed into the ER as cells progress to metaphase and are then released to reassemble the daughter Golgis at cytokinesis [40]. This model is based on the assumption that Golgi resident enzymes continuously cycle between the ER and Golgi during interphase, as suggested by live-cell imaging of GFP-fused proteins [27,40,58,59]. When ER export was blocked by the expression of a GDP-bound mutant of Sar1p, which arrests COPII vesicle budding, Golgi residents were seen to accumulate in the ER, resulting in Golgi disassembly [27,40,59]. During mitosis, the inhibition of ER export could result in similar entrapment of Golgi enzymes in the ER [40,58]. The inhibition of anterograde traffic with the continuation of retrograde trafficking would lead to a redistribution of Golgi enzymes to the ER, thus contributing to mitotic Golgi disassembly [59]. At the end of mitosis, the resumption of ER export would allow the reformation of new Golgis in the separating daughter cells [59]. Thus, this model suggests that the Golgi is not an autonomous organelle when it comes to inheritance and that it employs the ER for its partitioning [65]. However, this model has been criticized because the rate of recycling of Golgi components during interphase is too slow to explain their efficient relocation to the ER during the early stages of mitosis [55]. Whether mitosis affects the kinetics of retrograde transport remains unknown [58].

An alternative model maintains that the Golgi and ER remain as distinct compartments throughout mitosis, i.e., that they are inherited independently [40,66]. Rather than merging with the ER, the Golgi clusters instead break down by continuous budding of small COPI vesicles [40,66]. Depending on the cell type, the clusters and/or vesicles persist throughout mitosis and function as the partitioning units of the organelle [40,59,65]. This model is partly based on the finding that after BFA treatment and subsequent washout in the presence of a Sar1 mutant that inhibits COPII vesicle formation (thus blocking ER exit), Golgi matrix proteins (e.g., GRASPs) appear to be able to reform the Golgi independently of Golgi membrane proteins [56,65,67]. Furthermore, matrix protein-containing structures have been found to partition between the daughter cells during metaphase in the apparent absence of Golgi enzyme-containing membranes [65]. This suggests that Golgi matrix proteins serve as a scaffold for membranes containing Golgi residents and that independent partitioning of this matrix during metaphase ensures accurate Golgi reassembly at the end of mitosis [56,65]. The two models of Golgi partitioning are shown in **Figure 5** below.

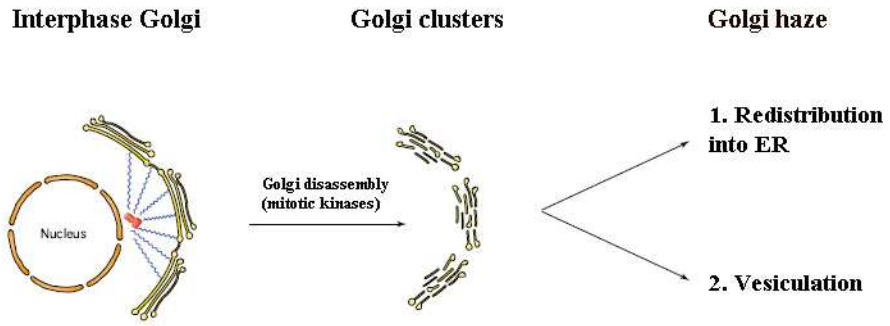

Figure 5. Two popular models of Golgi partitioning. As described in the text, the perinuclear Golgi ribbon of interphasic cells is disassembled into mitotic Golgi clusters by a process of ribbon unlinking and cisternal unstacking due to the phosphorylation of Golgi tethering factors by mitotic kinases. Golgi components present in these clusters are then either redistributed to the ER (1) or dispersed by COPI-mediated vesiculation (2), resulting in their characteristic diffuse localization ("Golgi haze") at metaphase. Figure modified from Reference [58].

During metaphase, matrix proteins and Golgi membranes have been observed to accumulate around the spindle poles, while the ER is excluded from the region of the spindle [54-56]. This suggests that the spindle machinery may be responsible for the partitioning of mitotic Golgi clusters [40,54,55,65,66]. Interestingly, the spindle has been found to be required for the partitioning of factors needed for Golgi ribbon reassembly, whereas components of polarized and functional Golgi stacks can be inherited independently of the spindle [56,66]. Overall, these findings suggest two distinct mechanisms of Golgi inheritance. Firstly, minimally functional Golgi stacks can be inherited in a spindle-independent manner [56,66] via a partitioning mechanism that depends on Brownian motion of Golgi matrix structures [55,65]. Golgi enzymes may either utilize the matrix structures to reach the daughter cells, or they may be partitioned via the ER, as described above for the alternative model [65]. Secondly, the spindle regulates the partitioning of additional factors that enable the linkage of Golgi stacks into a continuous ribbon [56].

1.5.3 Golgi reassembly

Golgi reassembly is essentially a reversal of the disassembly process, involving membrane fusion and cisternal restacking [40,59]. GM130 dephosphorylation at the end of mitosis results in the reformation of functional GM130-p115-giantin complexes, which mediate vesicle tethering and membrane fusion [40]. Following successful fusion events, p115 and GRASP65 can promote

restacking of cisternae and the linkage of individual stacks into a ribbon [40].

Golgi reassembly typically begins at telophase and results in the formation of two separate structures at opposite sides of the nucleus in each daughter cell [40,56,60]. The larger of these structures is positioned next to the centrosome at the distal side of the nucleus, while the smaller cluster is located in the midbody region between the forming cells, suggesting that the Golgi may have a role in the final abscission event during cytokinesis [40,56,60]. During the late stage of cytokinesis, the smaller Golgi cluster migrates to the opposite side of the nucleus and merges with the larger structure to form the final Golgi ribbon [40,60]. Notably, this coalescence is not synchronous, indicating that it may be related to other asynchronous events that take place during late cytokinesis (e.g., events affecting the centrosomes or cytoskeleton) [60].

1.5.4 Possible role of the IC in Golgi partitioning

In addition to the actin-based contractile ring, membrane traffic is known to be required for the separation of daughter cells during cytokinesis [40]. It has been suggested that the Golgi apparatus, as well as the recycling endosomes, contribute to the delivery of membranes to the cleavage furrow to facilitate the final abscission event [8,68]. However, cells are able to progress through mitosis in the presence of BFA, which results in Golgi disassembly [40]. Because the pcIC is a BFA-resistant structure that is functionally connected with the recycling endosomes [7], it could also function in membrane traffic events that result in the completion of cytokinesis. Furthermore, recent live-cell imaging studies of IC dynamics in GFP-Rab1A-expressing NRK cells have suggested a novel role of the IC in the partitioning of Golgi membranes during mitosis (M. Marie, H. Dale, N. Kouprina, J. Saraste, manuscript in preparation).

2 Aims

Recent live-cell imaging studies have shown that the IC persists during mitosis, suggesting that this compartment could participate in Golgi disassembly and the partitioning of Golgi components. Therefore, the overall goal of this master project was to further characterize the role of the IC in membrane traffic throughout the cell cycle, with a special focus on its lumenal acidification.

The following specific aims were set in order to study the role of the IC in protein trafficking in interphasic and mitotic cells:

1. To investigate how acidification inhibitors affect bidirectional trafficking at the ER-Golgi boundary during interphase.

2. To evaluate the effect of acidification inhibitors on the redistribution of Golgi enzymes during mitosis using mannosidase II (Man II) as a marker protein.

3. To obtain further insight on the mechanisms of Golgi partitioning during mitosis and the possible role of the IC in the redistribution of Golgi components.

3 Materials

Tables 1-17 provide a list of all reagents, solutions, cell lines, antibodies, drugs, technical equipment, software, and other materials used in the experiments.

3.1 Reagents

3.1.1 General

Table 1. Basic laboratory reagents used in the various experiments.

Reagent	**Abbreviation/Formula**	**Specifications**	**Supplier**
Disodium hydrogen phosphate dihydrate	$Na_2HPO_4 \cdot 2H_2O$	Pro-analysis grade (p.a.)	Merck, Darmstadt, Germany
Dulbecco's phosphate buffered saline	PBS	Modified without $CaCl_2$ and $MgCl_2$	Sigma-Aldrich, Steinheim, Germany
Ethanol	EtOH	Absolute	Sigma-Aldrich
Glucose (D (+)-glucose monohydrate)	-	-	Merck
Glycerol	-	99%	Sigma-Aldrich
Glycine	H_2NCH_2COOH	p.a.	Merck
Hydrochloric acid	HCl	-	Sigma-Aldrich
Hydroxyethylpiperazine ethanesulfonic acid	HEPES	Minimum 99.5%	Sigma-Aldrich
Methanol	MeOH	p.a.	Fluka, Buchs, Switzerland
MilliQ water	-	-	Millipore, Oslo, Norway
Paraformaldehyde	PFA	Reagent grade	Sigma-Aldrich
Potassium chloride	KCl	p.a.	Merck
Saponin	-	-	Sigma-Aldrich
Sodium chloride	NaCl	p.a.	Merck
Sodium dihydrogen phosphate monohydrate	$NaH_2PO_4 \cdot H_2O$	p.a.	Merck
Sodium hydroxide	NaOH	p.a.	Merck
Sucrose	$C_{12}H_{22}O_{11}$	-	Merck
Tris(hydroxymethyl)-amino methane	Tris	p.a.	Merck

3.1.2 Cell culture

Table 2. Reagents used in cell culture.

Reagent	Abbreviation	Specifications	Supplier
Dimethylsulphoxide	DMSO	-	Sigma-Aldrich
Dulbecco's modified Eagle's medium, 1x	DMEM	Containing 1 g/L D-glucose, L-glutamine, and sodium pyruvate	Gibco, Invitrogen, Grand Island, NY, USA
Fetal bovine serum	FBS	Heat inactivated	Gibco, Invitrogen
Ham's F12 nutrient mixture	F12	Containing L-glutamine	Gibco, Invitrogen
L-glutamine, 100x	L-glu	200 mM	Sigma-Aldrich
Penicillin-streptomycin, 100x	Pen-strep	5000 units/ml penicillin 5 mg/ml streptomycin	Sigma-Aldrich
Poly-L-lysine	-	Minimum 98%	Sigma-Aldrich
Trypsin-EDTA, 1x	-	-	Gibco, Invitrogen

3.1.3 Immunofluorescence and confocal imaging

Table 3. Reagents used in immunofluorescence and confocal imaging.

Reagent	Abbreviation	Specifications	Supplier
Bovine serum albumin	BSA	Fraction V ≥96%	Fluka
Goat serum	GS	Heat inactivated	Gibco, Invitrogen
Guanidine hydrochloride	Guanidine	>99.5%	Sigma-Aldrich
Sodium azide	Na-azide	-	Sigma-Aldrich
Vectashield® mounting medium	-	With DAPI	Vector Laboratories, Burlingame, CA, USA

3.1.4 Cell fractionation

Table 4. Reagents used in cell fractionation.

Reagent	Abbreviation	Specifications	Supplier
Complete Mini protease inhibitor cocktail	-	EDTA-free	Roche Diagnostics, Mannheim, Germany

Ethylenediamine tetraacetic acid	EDTA	99%	Sigma-Aldrich
Ethyleneglycerol tetraacetic acid	EGTA	Minimum 97%	Sigma-Aldrich
Hank's balanced salt solution	HBSS	-	Gibco, Invitrogen
OptiPrep™	-	Iodixanol 60% stock solution in H_2O	Axis-Shield AS, Oslo, Norway
Protease inhibitor cocktail (chymostatin, leupeptin, antipain, pepstatin)	CLAP	Stock solution containing 10 mg/ml of each	Sigma-Aldrich

3.1.5 SDS-PAGE

Table 5. Reagents used in SDS-PAGE.

Reagent	**Abbreviation**	**Specifications**	**Supplier**
Acrylamide/ bisacrylamide solution, 30%	-	Electrophoresis purity	Bio-Rad, Hercules, CA, USA
Ammonium persulfate	APS	For electrophoresis, ≥98% pure	Sigma-Aldrich
Beta-mercaptoethanol	-	Electrophoresis purity	Bio-Rad
Bromophenol blue	-	Electrophoresis purity	Bio-Rad
N,N,N',N'-tetramethylethylene diamine	TEMED	-	Bio-Rad
Ponceau S	-	-	Fluka
Precision Plus™ protein standard	-	-	Bio-Rad
Sodium dodecylsulfate	SDS	Electrophoresis purity	Bio-Rad

3.1.6 Western blotting

Table 6. Reagents used in Western blotting.

Reagent	**Supplier**
Difco™ nonfat dry milk	Becton Dickinson, Sparks, MD, USA
Supersignal®WestPico Chemiluminescent Substrate	Thermo Fisher Scientific, Rockford, IL, USA
Tween®20	Sigma-Aldrich

3.2 Solutions

3.2.1 Immunofluorescence

Table 7. Solutions for immunofluorescence.

Solution	Abbreviation	Total volume	Components	Special instructions
0.2 M phosphate buffer, pH 7.2	-	100 ml	28 ml of 0.2 M $NaH_2PO_4 \cdot H_2O$ (27.6 g in 1 L dH_2O) 72 ml of 0.2 M $Na_2HPO_4 \cdot 2H_2O$ (35.6 g in 1 L dH_2O)	Adjust pH to 7.2.
Paraformaldehyde, 3% (w/v)	3% PFA	100 ml	3 g of PFA 50 ml of dH_2O 50 ml of 0.2 M phosphate buffer	Add 5 drops of NaOH and warm solution to 60°C under constant mixing until clear. Add phosphate buffer and filter solution. Store at 4°C.
Washing buffer (1x PBS with 0.2% (w/v) BSA and Na-azide)	WB	400 ml	400 ml of 1x PBS 800 mg of BSA 400 µl of Na-azide	Store solution at 4°C.
Washing buffer + 0.2% (w/v) saponin	WBS	200 ml	400 mg of saponin 200 ml of WB	Filter solution and store at 4°C.
Blocking buffer (5% (v/v) goat serum + WBS)	BB	10 ml	500 µl of goat serum 10 ml of WBS	Filter solution using syringe capped with sterile filter (0.22 µm pore size) and store at 4°C.

3.2.2 Cell fractionation

Table 8. Solutions for cell fractionation.

Solution	Total volume	Components	Special instructions
1 M Tris-HCl, pH 7.5	1 L	121.1 g of Tris 800 ml of dH_2O	Adjust pH to 7.5 with HCl. Bring volume to 1 L with dH_2O. Store at 4°C.

Homogenization buffer (for OptiPrep™) (130 mM KCl, 25 mM NaCl, 1 mM EGTA, 25 mM Tris-HCl, pH 7.5)	200 ml	5 ml of 1 M NaCl (57.3 g in 1 L dH_2O) 5 ml of 1 M Tris-HCl, pH 7.5 1.94 g of KCl 76 mg of EGTA	Bring volume to 200 ml with dH_2O.
Washing buffer (for OptiPrep™) (140 mM NaCl, 30 mM KCl, 10 mM EDTA, 25 mM Tris-HCl, pH 7.5)	200 ml	28 ml of 1 M NaCl 5 ml of 1 M Tris-HCl, pH 7.5 447 mg of KCl 1.17 g of EDTA	Bring volume to 200 ml with dH_2O.
HEPES-EDTA buffer, pH 7.4 (10 mM HEPES, 1 mM EDTA)	200 ml	477 mg of HEPES 117 mg of EDTA	Bring volume to 200 ml with dH_2O. Adjust pH to 7.4 with HCl.
Homogenization buffer (for glycerol gradients) (50 mM NaCl, 10 mM HEPES, 1 mM EDTA, pH 7.4)	200 ml	10 ml of 1 M NaCl	Bring volume to 200 ml with HEPES-EDTA buffer, pH 7.4.
Washing buffer (for glycerol gradients) (250 mM sucrose, 10 mM HEPES, 1 mM EDTA, pH 7.4)	200 ml	17.1 g of sucrose	Bring volume to 200 ml with HEPES-EDTA buffer, pH 7.4.

3.2.3 SDS-PAGE

Table 9. Solutions for SDS-PAGE.

Solution	**Total volume**	**Components**	**Special instructions**
0.5 M Tris-HCl, pH 6.8	100 ml	6 g of Tris 60 ml of dH_2O	Adjust pH to 6.8 with HCl. Bring volume to 100 ml. Store at 4°C.
1.5 M Tris-HCl, pH 8.8	150 ml	27.23 g of Tris 80 ml of dH_2O	Adjust pH to 8.8 with HCl. Bring volume to 150 ml. Store at 4°C.
SDS, 10% (w/v)	100 ml	10 g of SDS 90 ml of dH_2O	Bring volume to 100 ml.
APS, 10% (w/v)	1 ml	100 mg of APS	Dissolve in 1 ml of dH_2O.

10% resolving gel	10 ml (for 2 gels)	4.1 ml of dH_2O 2.5 ml of 1.5 M Tris-HCl, pH 8.8 3.3 ml of 30% acrylamide/bis 0.1 ml of 10% SDS 50 µl of 10% APS 5 µl of TEMED	Add 10% APS and TEMED immediately prior to pouring the gel.
4% stacking gel	10 ml (for 2 gels)	6.1 ml of dH_2O 2.5 ml of 0.5 M Tris-HCl, pH 6.8 1.3 ml of 30% acrylamide/bis 0.1 ml of 10% SDS 50 µl of 10% APS 10 µl of TEMED	Add 10% APS and TEMED immediately prior to pouring the gel.
10x electrophoresis buffer	1 L	30.3 g of Tris 144 g of glycine 10 g of SDS 800 ml of dH_2O	Adjust volume to 1 L with dH_2O. Store at 4°C.
1x electrophoresis buffer (25 mM Tris, 192 mM glycine, 0.1% SDS)	1 L	100 ml of 10x electrophoresis buffer	Adjust volume to 1 L with dH_2O.
Sample buffer, 2x	10 ml	3.55 ml of dH_2O 1.25 ml of 1 M Tris-HCl, pH 6.8 2.5 ml of glycerol 2.0 ml of 10% SDS 0.2 ml of 0.5% (w/v) bromophenol blue	Add 50 µl of beta-mercaptoethanol prior to use.

3.2.4 Western blotting

Table 10. Solutions for Western blotting.

Solution	Abbreviation	Total volume	Components	Special instructions
1 M Tris-HCl, pH 7.5	-	1 L	121.1 g of Tris 800 ml of dH_2O	Adjust pH to 7.5 with HCl. Bring volume to 1 L with dH_2O. Store at 4°C.
Transfer buffer (25 mM Tris, 190 mM glycine, 10% methanol)	-	1 L	3.03 g of Tris 14.4 g of glycine 100 ml of MeOH 500 ml of dH_2O	Adjust volume to 1 L with dH_2O.

Washing buffer (20 mM Tris-HCl, pH 7.5, 150 mM NaCl, 0.1% Tween)	TBS-Tween	1 L	20 ml of 1 M Tris-HCl, pH 7.5 150 ml of 1 M NaCl (57.3 g in 1 L dH_2O) 1 ml of Tween® 20	Adjust volume to 1 L with dH_2O.
Blocking buffer (5% (w/v) milk/TBS-Tween)	-	100 ml	5 g of nonfat dry milk 80 ml of TBS-Tween	Adjust volume to 100 ml with TBS-Tween.

3.3 Cell lines

Table 11. Cell lines used in the experiments.

Cell line	**Abbreviation**	**Supplier**
Baby hamster kidney cells expressing triple hemagglutinin (HA)-tagged wildtype CFTR	BHK WT-CFTR	M. Sharma, Reference [69]
Normal rat kidney cells	NRK parental	ATCC
NRK GFP-Rab1A cells	NRK GFP-Rab1A	M. Marie, Reference [7]

3.4 Antibodies

3.4.1 Antibodies for immunofluorescence

Antibody incubations were carried out for 2 hours at RT, unless otherwise indicated. The secondary antibodies were Texas Red (TxR) and fluorescein isothiocyanate (FITC) conjugates.

Table 12. Antibodies used in immunofluorescence.

Antibody	**Stock concentration**	**Dilution**	**Source**
Mouse anti-HA tag	1 mg/ml	1:100	Nordic Biosite, Copenhagen, Denmark
Mouse anti-Man II	5-7 mg/ml	1:250 (3% PFA + 6 M guanidine - 5 min or methanol fix)	Nordic Biosite
Rabbit anti-β-COP	4.4 mg/ml	1:500	Affinity Bioreagents, Golden, Colorado, USA

Rabbit anti-Man II	Serum	1:250	Kelley Moremen, University of Georgia, Athens, Georgia, USA
Rabbit anti-p58	Serum	1:200	Randy Schekman, Univesity of California, Berkeley, CA, USA
Rabbit anti-p58	Purified IgG	1:20	Affinity purified from serum, Reference [70]
Rabbit anti-Rab1	Purified IgG	1:20 o/n	Affinity purified from serum, Bruno Goud, Institute Curie, Paris, France
FITC-coupled goat anti-mouse IgG	2 mg/ml	1:50	Jackson Immuno Research, West Grove, PA, USA
FITC-coupled goat anti-rabbit IgG	2 mg/ml	1:50	Jackson Immuno Research
TxR-coupled goat anti-mouse IgG	2 mg/ml	1:50	Jackson Immuno Research
TxR-coupled goat anti-rabbit IgG	2 mg/ml	1:50	Jackson Immuno Research

3.4.2 Antibodies for Western blotting

Table 13. Antibodies used in Western blotting.

Antibody	**Stock concentration**	**Dilution**	**Source**
Rabbit anti-Man II	Serum	1:500 (o/n)	Kelley Moremen
Rabbit anti-p58	Serum	1:5000 (o/n)	Randy Schekman
Rabbit anti-Rab1	Purified IgG	1:500 (o/n)	Bruno Goud
HRP-coupled goat anti-rabbit IgG (light chain specific)	0.8 mg/ml	1:5000 (2 h)	Jackson Immuno Research

3.5 Drugs

Table 14. Drugs used in the experiments.

Product	**Abbreviation/Formula**	**Specifications**	**Supplier**
Ammonium chloride	NH_4Cl	≥99.5%	Sigma-Aldrich
Bafilomycin A1	Baf A1	≥90% from *Streptomyces griseus*	Sigma-Aldrich

Brefeldin A	BFA	>99% from *Eupenicillium brefeldianum*	Epicentre Biotechnologies, Madison, WI, USA
Chloroquine diphosphate salt	CQ	-	Sigma-Aldrich
Cycloheximide	CHX	-	Calbiochem, Darmstadt, Germany
Monensin sodium salt	-	-	Sigma-Aldrich

3.6 Technical equipment

Table 15. Technical equipment used in the experiments.

Instrument	**Specifications**	**Supplier**
Ball bearing cell cracker (homogenizer)	Ball size 8.010 mm	EMBL Precision Engineering, Heidelberg, Germany
Beckman swinging bucket rotor	SW41	Beckman, Palo Alto, CA, USA
Beckman ultracentrifuge	Optima™ LE-80K TL-100	Beckman
Benchtop centrifuge	5810, 5810 R	Eppendorf, Hamburg, Germany
Biofuge	-	Heraeus Instruments, Germany
Confocal Leica TCS SP2 AOBS	63x objective	Leica Microsystems, Wetzlar, Germany
Electrophoresis power supply	PowerPac 300	Bio-Rad
Horizontal shaker	MMPV 15	Heto-Holten AS, Allerød, Denmark
Inverted light microscope	Olympus CKX31	Olympus, UK
Liquid nitrogen tank	Locator 8	Thermo Fisher Scientific
Luminescent Image Analyzer	LAS-3000	Fujifilm, Tokyo, Japan
Milli-Q Ultrapure water purification system	-	Millipore, Oslo, Norway
Mini Protean® 3 Cell Electrophoresis Module	-	Bio-Rad
Mini Trans-Blot® Electrophoretic Transfer Cell	-	Bio-Rad
Steri-cycle CO_2 incubator	With HEPA filter	Thermo Forma, Marietta, OH, USA
Thermomixer	-	Eppendorf
Water bath	-	Stuart Scientific, UK

3.7 Software

Table 16. Software used for data analysis and image composition.

Program	Specifications	Supplier
Excel	Microsoft Office X for Macintosh	Microsoft, Redmond, WA, USA
ImageJ	-	NIH, Bethesda, MD, USA
Image Reader LAS-3000	Version 2.2	Fujifilm
Leica LAS Image Analysis	-	Leica Microsystems
Photoshop	Version 7.0.1	Adobe Photoshop, San Jose, CA, USA

3.8 Other materials

Table 17. Other materials used in the experiments.

Product	Specifications	Supplier
Cell culture dishes	6-well, 12-well	MedProbe, Oslo, Norway
Cell culture flasks	25 cm², 75 cm², 300 cm²	MedProbe
Cell scraper	25 cm	Sarstedt, Germany
Centrifuge tubes	500 µl, 1.5 ml	Eppendorf
Centrifuge tubes	15 ml, 50 ml	Sarstedt
Circular glass coverslips	18 mm Ø Thickness 0.17 ± 0.01 mm	Chemi-Teknik AS, Oslo, Norway
Comb	-	Bio-Rad
Cryotubes	-	Nunc, Denmark
Fiber pads	-	Bio-Rad
Microscopic objective slides	76 x 26 mm	Chemi-Teknik AS
Nitrocellulose membrane	0.2 µm pore size	Schleicher & Schuell, Dassel, Germany
Outer glass plate, 1 mm	Mini Protean® 3	Bio-Rad
pH indicator strips	pH 5-10	Merck
Short plate	Mini Protean® 3	Bio-Rad
Syringe, Plastipak™	10 ml	Becton Dickinson SA, Madrid, Spain
Syringe filter, Acrodisc®	25 mm with 0.2 µm HT Tuffryn® membrane	Pall Corporation, Ann Arbor, MI, USA
Ultra-clear centrifuge tubes	SW41	Beckman
Whatman filter paper	0.92 mm thickness	Whatman, England

4 Methods

The methods described in the following section were employed in experiments involving 3 different cell lines. Refer to Materials (Section 3) for preparation of various solutions.

4.1 Cell culture

All cell culture work, including drug treatments and experimental manipulations, was performed under sterile conditions. All solutions used for the procedures described were either sterilized before use or purchased as sterile.

4.1.1 General maintenance

Cultured cells (NRK parental, NRK GFP-Rab1A) were grown to 70-90% confluency in 25 cm² or 75 cm² polystyrene culture flasks equipped with filter caps. Cells were grown in an incubator at 37ºC and 5% CO_2 in DMEM supplemented with 10% heat inactivated FBS, 50 IU/ml penicillin, 50 µg/ml streptomycin, and 2 mM L-glutamine. BHK WT-CFTR cells were grown in 1:1 DMEM and F12 medium supplemented with 5% heat inactivated FBS, 50 IU/ml penicillin, 50 µg/ml streptomycin, and 2 mM L-glutamine.

4.1.2 Thawing of cells

Cells stored in liquid nitrogen (-196ºC) were retrieved from the nitrogen tank and thawed initially under running tap water and further thawed on ice for approximately 5 min. The cell suspension (1 ml) was then transferred into a 15 ml centrifuge tube containing 9 ml of pre-cooled (4°C) complete culture medium, and the solution was centrifuged at 1000 rpm for 5 min in a bench top centrifuge. After centrifugation, the DMSO-containing supernatant was removed by suction, and the cells were resuspended in 5 ml of fresh pre-warmed (37°C) medium and plated in 25 cm² culture flasks at the appropriate dilution. The culture flasks were then transferred to the CO_2 incubator.

4.1.3 Passage of cells

The cells were routinely passaged (every 2-3 days) after reaching approximately 70-90% confluency, as determined by examination with a light microscope using phase contrast optics. Cells were washed once with 3-5 ml of PBS, and 0.5-1 ml of pre-warmed (37°C) trypsin-EDTA was added. The cells were then incubated in the CO_2 incubator for approximately 3 min in order to allow the cells to partially detach; detached cells have a characteristic round appearance when observed under a light microscope. The cells were completely detached from the substratum by hitting the side of the flask several times. 5 ml of fresh medium were then added to the cells, and the cell aggregates were disrupted by pipetting the cell suspension up and down a few times. The cell suspension was then diluted 1:5, 1:10, 1:20, or other dilution variations in fresh pre-warmed (37°C) culture medium and resuspended to ensure an even distribution.

4.1.4 Freezing of cells

Cells growing in 25 cm² culture flasks were amplified, trypsinized, and resuspended in growth medium, as previously described. Cell suspensions were then centrifuged for 5 min at 1000 rpm, and the supernatant was removed by suction. The cell pellet was resuspended in ice-cold 1:10 DMSO-containing medium, and the suspension was aliquoted at 1 ml into labeled cryotubes. DMSO is a cryoprotectant that prevents cellular rupture at low temperatures. The tubes were placed for 3 hours in the -20°C freezer, followed by overnight freezing at -80°C. The next day, the tubes were transferred to the liquid nitrogen tank for storage.

4.1.5 Plating of cells on coverslips

Pre-washed glass coverslips were placed into 6- or 12-well culture dishes and allowed to dry. Cell suspensions were obtained as previously described and diluted in complete medium (e.g., 1:10). 2 ml volumes were added to each well. The cells were allowed to grow for at least 24 h prior to beginning experiments in order to reach confluency.

In the case of mitotic shake-offs (described in Section 4.2.2), coverslips were coated with 100 µl of poly-L-lysine (diluted 1:10 in dH_2O) for 10 min and subsequently washed 3x with sterile dH_2O. 100 µl of cell suspensions were added to the coverslips, and the cells were allowed to bind on ice for approximately 10 min prior to fixation or further manipulation.

4.2 Experimental manipulations

4.2.1 Drug treatments

The following treatments listed in **Table 18** were used for cells at 70-90% confluency, grown on coverslips in culture dishes or in culture flasks at 37°C in complete DMEM.

Table 18. Drugs used in the experiments.

Drug	**Abbreviation/Formula**	**Stock concentration**	**Working concentration**
Ammonium chloride	NH_4Cl	1 M stock in H_2O	10 mM (1:100)
Bafilomycin A1	Baf A1	100 μM stock in EtOH	0.5 μM (1:200)
Brefeldin A	BFA	5 mg/ml stock in EtOH	5 μg/ml (1:1000)
Chloroquine	CQ	10 mM stock in H_2O	100 μM (1:100)
Cycloheximide	CHX	10 mg/ml stock in PBS	50 μg/ml (1:200)
Monensin	-	1 mM stock in EtOH	1 μM (1:1000)

4.2.2 Mitotic shake-offs

Mitotic shake-offs were done in order to collect and concentrate the mitotic cells on coverslips for easier identification and quantification. Drug treatments were conducted as shown in **Table 18** and done prior to the shake-offs (i.e., done in culture flasks at 70-90% confluency). Mitotic cells were released by hitting the side of the flask, followed by examination under a light microscope. The cell suspensions containing the mitotic cells were collected, placed on ice, and centrifuged for 5 min at 1000 rpm. After centrifugation, the supernatant was removed by suction, and the cell pellets were resuspended in 100-200 μl of complete medium or HBSS. 100 μl of cell suspension were added to coverslips pre-coated with poly-L-lysine on ice, as described in Section 4.1.5. Alternatively, cell suspensions of mitotic cells were subjected to cell fractionation techniques (see Section 4.4).

4.2.3 Low temperature treatments

Low temperature treatments were performed with steady state cultures grown in culture flasks, as well as with mitotic shake-offs. For the steady state cultures, the medium was replaced with medium containing 20 mM HEPES, pH 7.2 pre-cooled to 15°C in a water bath. The culture flasks were then incubated in a 15°C water bath. Mitotic shake-offs were performed immediately following low temperature incubation in order to collect the mitotic cells, which were then plated on poly-L-lysine-coated coverslips. Alternatively, mitotic cells were collected prior to low temperature incubation, plated on coverslips, and then subjected to low temperature treatment. For cell fractionation studies, cell suspensions containing mitotic cells were transferred into 50 ml tubes and pelleted at 1000 rpm for 5 min. The pellets were then resuspended in 50 ml total of medium containing 20 mM HEPES, pH 7.2 pre-cooled in a 15°C water bath. The samples were incubated at 15°C and then centrifuged at 1000 rpm for 5 min in a pre-cooled (4°C) centrifuge. The pellets were resuspended in 10 ml of ice-cold HBSS and processed for cell fractionation and velocity sedimentation in Opti-Prep™ gradients as described in Section 4.4.2.

4.3 Immunofluorescence staining and confocal microscopy

4.3.1 Principle

Immunofluorescence microscopy is a technique used to detect proteins in tissue samples and cultured cells. Samples are first incubated with purified antibodies that recognize particular epitopes, and the primary antibodies are in turn recognized by secondary antibodies coupled to fluorescent dyes (e.g., FITC). The protein of interest is then localized by excitation of the fluorescent molecule with an appropriate wavelength of light, followed by detection of the emission signal. Double-labeling immunofluorescence can be used to compare the distribution of two different proteins in a cell by using two secondary antibodies coupled to different fluorescent dyes.

Confocal microscopy is a special type of fluorescence microscopy that has high resolution and optimal contrast. **Figure 6** highlights the basic components of a confocal microscope. The unique feature is the presence of two pinholes that allow transmitted light to be focused. As shown in the figure, the laser beam passes through an illuminating aperture prior to reaching the surface of the specimen so that only a small portion of the sample is illuminated. In turn, the emitted

fluorescence passes through a confocal aperture prior to reaching the photodetector in order to reject out-of-focus light. The composite image is then displayed on a computer screen.

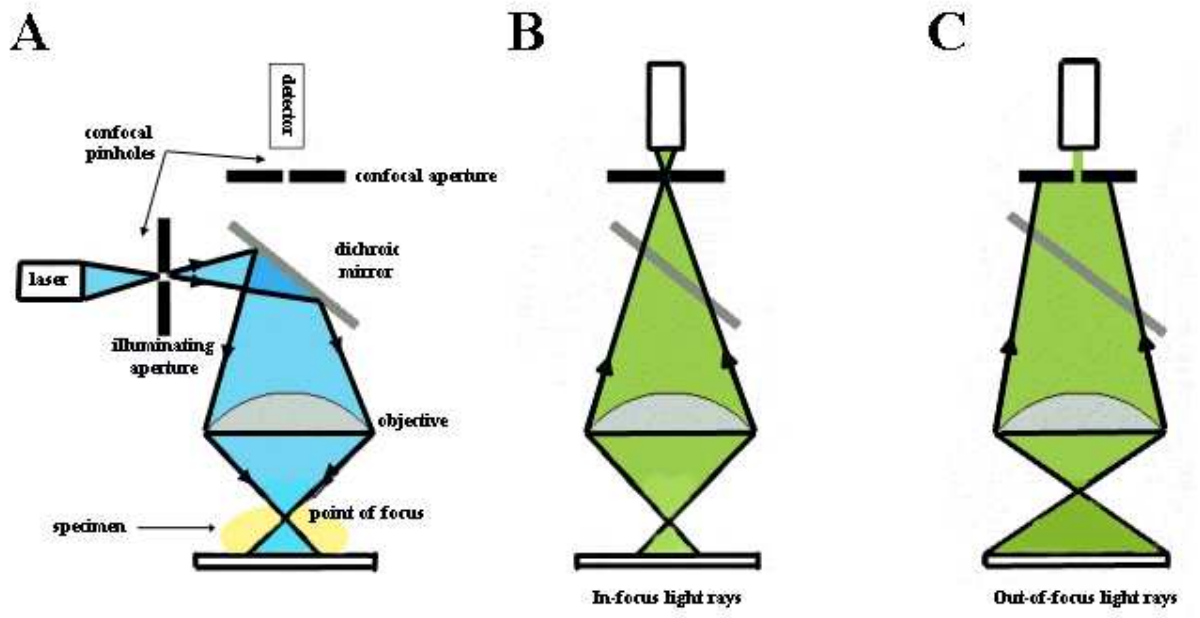

Figure 6. Principles of confocal fluorescence microscopy. (A) The basic components of a confocal microscope are illustrated in the figure. Note the presence of two confocal pinholes. The illuminating aperture ensures that only a small part of the specimen is illuminated by the laser by focusing the beam on the specimen surface. The emitted fluorescence reaches the photodetector by passing through a dichroic mirror. The presence of a confocal aperture ensures that only in-focus light reaches the detector (B), while out-of-focus light is excluded (C). This contributes to the high resolution and contrast of confocal fluorescence microscopy. Figure modified from Reference [6].

4.3.2 Sample preparation

As described in Section 4.1.5, samples were plated on coverslips at least 24 h prior to the start of the experiment and allowed to reach a confluency of 70-90%. After the treatments (see Section 4.2), cells were fixed for 30-60 min at RT with 1 ml of 3% PFA prepared in 0.1 M phosphate buffer, pH 7.2. After fixation, the cells were washed 2x with 2 ml of washing buffer (PBS containing 0.2% BSA) and permeabilized/blocked for at least 15 min in 1 ml of blocking buffer (5% goat serum, 0.2% saponin, 0.2 % BSA in PBS). The cells were then incubated at RT with 40 µl of pre-cleared (5 min, 13000 rpm in a biofuge) primary antibody diluted in blocking buffer (see Section 3.4.1, **Table 12** for the appropriate dilutions and durations). The primary antibody was removed by washing 2x with washing buffer containing 0.2% saponin (2 ml), followed by a third time for 2 h. The secondary antibody (FITC- or TxR-conjugated goat anti-rabbit or -mouse

fragment antigen binding (F(ab)) fragment) was diluted 1:50 in blocking buffer and pre-cleared; 40 µl were added to the coverslips for 2 h. The secondary antibody was then washed out as described overnight. Finally, the cells were washed 1x with PBS and mounted onto objective slides using Vectashield® mounting medium containing DAPI.

Alternatively, cells were fixed for 10 min at -20°C with 1 ml of pre-cooled methanol (-20°C) and washed extensively on ice with washing buffer (PBS containing 0.2% BSA). The samples were subsequently incubated with primary and secondary antibodies diluted in blocking buffer without saponin. **Table 12** (Section 3.4.1) describes the specific fixation protocols for each antibody used. The samples were mounted as described.

4.3.3 Image acquisition

The cells were examined using a Leica TCS SP2 AOBS confocal system equipped with a 63x/1.4 NA Plan Apochromat oil immersion objective, ~1.2 airy unit pinhole aperture, and appropriate filter combinations. The lasers used were blue diode (405 nm - DAPI), argon/krypton (488 nm - GFP and FITC/514 nm - YFP), and helium neon (594 nm - TxR) lasers. When visualizing samples double-stained with two fluorophores, the presence of cross-excitation and -emission was verified prior to imaging. This was done by testing one laser at a time, and if both emission signals appeared, the fluorophores were determined to be cross-emitting. In order to avoid this, the sequential scanning mode was then selected. For imaging and quantification, a representative area was randomly selected from the whole area of the coverslip. After the images were acquired, they were further processed using Adobe Photoshop version 7.0 or analyzed using standard Leica confocal software (see Section 4.7).

4.4 Cell fractionation

All steps were performed on ice using pre-cooled solutions, and all centrifugations were performed at 4°C. An overview of the procedure is presented in **Figure 7**. This method was an adaptation for NRK cells from a protocol developed for PC12 cells [71].

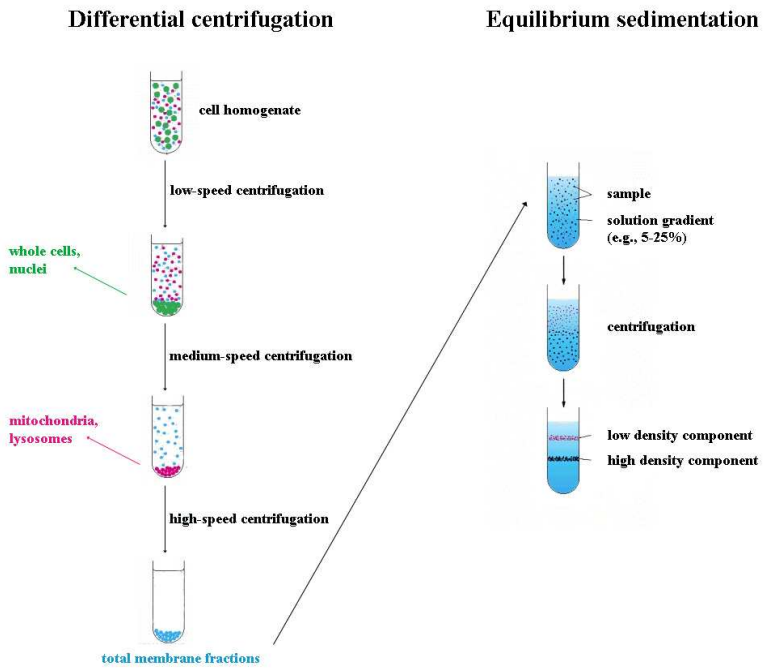

Figure 7. Overview of cell fractionation. See text below for more details. Figure modified from Reference [6].

4.4.1 Principle

Cell fractionation is a method that allows for the separation of organelles from a population of cells. It consists of two principal steps, which must be performed at cold temperatures in order to minimize damage to molecules from cellular enzymes. The first step is the homogenization of cells using a homogenizer, which breaks cellular membranes and releases organelles. The next step is purification, which is accomplished by differential centrifugation and/or equilibrium sedimentation. Differential centrifugation involves a sequential increase in gravitational force that results in the sequential separation of organelles as a function of their density. Larger and denser structures pellet at lower centrifugal forces, whereas smaller organelles remain in the supernatant. As a result, one can sequentially isolate and remove whole cells, nuclei, mitochondria, lysosomes, etc. The resulting total membrane fractions can be further separated by equilibrium sedimentation, which relies on solution gradients (e.g., glycerol) in order to separate structures based on their individual densities. Upon centrifugation, each organelle settles in a gradient comparable to its own density; this allows ultraprecise separation of structures.

4.4.2 Experimental protocol using iodixanol gradients (Opti-Prep™)

4.4.2.1 Homogenization of cells

The following protocol is described for parental NRK cells grown to 70-90% confluency in ten 300 cm^2 culture flasks and passaged the previous day. After the treatments (see Section 4.2), mitotic cells were collected by shake-off (see Section 4.2.2) into 50 ml tubes. The cells were pelleted at 1000 rpm for 5 min in a pre-cooled (4°C) bench top centrifuge, and the pellets were resuspended in 10 ml of HBSS. The suspensions were combined into two 50 ml tubes and each filled to 50 ml with HBSS. The cells were pelleted again, and the pellets were resuspended in 15 ml total of washing buffer (140 mM NaCl, 30 mM KCl, 10 mM EDTA, 25 mM Tris-HCl, pH 7.4). The samples were centrifuged as before and resuspended in 0.5-1 ml of homogenization buffer (130 mM KCl, 25 mM NaCl, 1 mM EGTA, 25 mM Tris-HCl, pH 7.4) supplemented with protease inhibitors (1x CLAP and 1 tablet of Complete Mini per 10 ml of buffer). The pellets were kept on ice.

The cell homogenizer equipped with a 8.010 mm diameter stainless steel ball in its chamber was assembled as previously described in Reference [71] and washed with homogenization buffer before use. The cell suspension was passed through the homogenizer approximately 20-30 times by pressing the pistons of the two attached 1 ml syringes. Samples of the cell suspension before and after homogenization were viewed using phase contrast optics in an inverted microscope (20-40x) in order to ensure that the cells were homogenized adequately. The homogenates were then centrifuged at 600 x g for 10 min at 4°C to pellet the nuclei and cell debris. The post-chromosomal supernatants were recovered into a 1.5 ml Eppendorff tube and kept on ice.

4.4.2.2 Preparation of iodixanol gradients and equilibrium sedimentation

The iodixanol gradients were prepared immediately prior to centrifugation as detailed in **Table 19** by mixing varying volumes of homogenization buffer (without protease inhibitors) and 50% iodixanol (Opti-Prep™) stock solution. The gradients were obtained by carefully pipetting the different mixtures on top of each other from highest to lowest concentration (1.2 ml of each) into a SW41 ultracentrifuge tube. 0.8 ml of sample was then pipetted on top of each gradient. The tubes were balanced to 0.1 g accuracy and centrifuged at 4°C for 30 min at 150,000 x g in the Beckman LE-80K ultracentrifuge using the SW41 rotor. After centrifugation, 8 fractions (~1.2 ml

each) were collected from the top and diluted with homogenization buffer up to 11.5 ml. The fractions were then centrifuged for 1 h at 100,000 x g in the ultracentifuge. After centrifugation, the supernatant was removed, and the pellets containing the membranes were resuspended in 50-100 µl of homogenization buffer supplemented with protease inhibitors and frozen in 10-20 µl aliquots at -80°C. The samples were subsequently analyzed by SDS-PAGE and Western blotting (see Sections 4.5 and 4.6).

Table 19. Preparation of 5-25% iodixanol gradients.

% iodixanol	50% iodixanol	Homogenization buffer
5%	0.50 ml	4.50 ml
7.5%	0.75 ml	4.25 ml
10%	1.00 ml	4.00 ml
12.5%	1.25 ml	3.75 ml
15%	1.50 ml	3.50 ml
17.5%	1.75 ml	3.25 ml
20%	2.00 ml	3.00 ml
22.5%	2.25 ml	2.75 ml
25%	2.50 ml	2.50 ml

4.4.3 Experimental protocol using glycerol gradients

4.4.3.1 Homogenization of cells

Each gradient was prepared from mitotic shake-offs (see Section 4.2.2) of parental NRK cells grown to 70-90% confluency in eight 300 cm² culture flasks. The cells were passaged the previous day into complete DMEM containing high glucose (4500 mg/L) in order to increase the mitotic index. Following treatments (see Section 4.2), the mitotic cells were collected by shake-off and pipetted into 50 ml tubes on ice. Cells were pelleted by centrifugation for 5 min at 1000 rpm. The cells were then washed with HBSS by first resuspending each pellet in 5 ml of HBSS and then combining the pellets from each condition into a corresponding 50 ml tube. The tubes were filled to 50 ml with HBSS and centrifuged for 5 min at 1000 rpm. The pellets were then resuspended in 5 ml of washing buffer (250 mM sucrose in HEPES-EDTA buffer, pH 7.4) and

transferred to 15 ml tubes. Washing buffer was added to yield a final volume of 15 ml. The cells were then centrifuged again for 5 min at 1000 rpm. The supernatant was discarded, and the pellets were kept on ice. The procedure was repeated for a second shake-off from the flasks.

The pellets were resuspended in 0.5-1 ml of homogenization buffer (50 mM NaCl, 10 mM HEPES, 1 mM EDTA, pH 7.4 supplemented with Complete Mini and 1x CLAP) and combined with the corresponding pellet from the second shake-off, followed by homogenization (see Section 4.4.2.1). The homogenates were then centrifuged at 600 x g for 10 min at 4°C. The post-chromosomal supernatants were recovered into 1.5 ml Eppendorff tubes and kept on ice.

4.4.3.2 Preparation of glycerol gradients and equilibrium sedimentation

50% glycerol (in HEPES-EDTA buffer, pH 7.4) was mixed with HEPES-EDTA buffer in order to make solutions for each of the 5-25% glycerol gradients (see **Table 20**).

Table 20. Preparation of 5-25% glycerol gradients.

% glycerol	**50% glycerol**	**HEPES-EDTA buffer**
5%	0.50 ml	4.50 ml
7.5%	0.75 ml	4.25 ml
10%	1.00 ml	4.00 ml
12.5%	1.25 ml	3.75 ml
15%	1.50 ml	3.50 ml
17.5%	1.75 ml	3.25 ml
20%	2.00 ml	3.00 ml
22.5%	2.25 ml	2.75 ml
25%	2.50 ml	2.50 ml

0.8 ml of 80% (w/v) sucrose (in HEPES-EDTA buffer, pH 7.4) was added to the bottom of two SW41 ultracentrifuge tubes. The gradients were prepared by sequential pipetting (1.1 ml) of the glycerol solutions on top of each other from highest to lowest concentration. 0.8 ml of sample was then carefully pipetted on top of each gradient, and the tubes were balanced to 0.1 g accuracy. Velocity gradient centrifugation was carried out in a Beckman SW41 rotor at 150,000 x

g for 30 min at 4°C.

After centrifugation, 9 fractions (~1.2 ml each) were collected from the top and each diluted to 11.5 ml with ice-cold PBS in separate ultracentrifuge tubes. The separate fractions were centrifuged for 60 min at 100,000 x g in the SW41 rotor in order to concentrate the membranes. The membrane pellets were resuspended in 50-100 µl of homogenization buffer supplemented with Complete Mini and 1x CLAP. The resuspended membranes were then divided into 10-20 µl aliquots and frozen at -80°C to be subsequently analyzed by SDS-PAGE and Western blotting (see Sections 4.5 and 4.6).

4.5 Sodium dodecyl sulfate polyacrylamide gel electrophoresis (SDS-PAGE)

SDS-PAGE was used in order to separate proteins present in membrane fractions obtained by cell fractionation, as described in Section 4.4.

4.5.1 Principle

SDS-PAGE is a technique that allows for the separation of proteins in an applied electric field based on size; the proteins can be subsequently visualized by staining or further analyzed by immunoblotting. Acrylamide provides a support matrix for protein migration and forms a porous gel upon polymerization in the presence of a cross-linking reagent (bisacrylamide). The percentage of acrylamide in a gel determines the pore size, which affects the migration of proteins through the gel. A high polyacrylamide concentration allows the gel to separate smaller proteins, while a low concentration allows for the separation of larger molecules.

Because proteins are amphoteric compounds that may have a net positive or negative charge depending on the pH of the solution, overall protein separation is determined by both size and charge. However, treatment with an anionic detergent such as SDS denatures proteins and gives them a uniform charge per unit length so that they migrate toward the positive electrode in an electric field based on their molecular size.

4.5.2 Sample preparation

The following protocol is described for the Mini Protean® 3 Cell Electrophoresis Module from Bio-Rad. Cell fractionation samples were diluted in 1:2 in sample buffer (see Section 3.2.3, **Table 9**). Samples were then boiled for 5 min at 95°C (or 15 min at 56°C) in a thermomixer before loading onto the gel.

4.5.3 Electrophoresis

The Mini Protean® 3 Cell Electrophoresis Module (Bio-Rad) was assembled according to the instruction manual, and the 1 mm thick gel was prepared immediately prior to use. The thick gel consisted of a resolving gel and an overlying stacking gel (see Section 3.2.3, **Table 9**). The resolving gel was poured in between the glass plates and allowed to polymerize for 45-60 min before adding the stacking gel. The purpose of the stacking gel was to concentrate the protein sample into a sharp band before entering the resolving gel. 20 µl of each sample and 10 µl of Precision Protein Standard™ (Bio-Rad) containing a mixture of pre-stained markers were then loaded into the appropriate wells. Electrophoresis was carried out in 1x electrophoresis buffer (0.1% SDS, 25 mM Tris, 192 mM glycine). The gel was run for ~45 min at 200 V. The resolving gel was then incubated for 10 min in transfer buffer containing 10% methanol prior to transfer to a nitrocellulose membrane (Section 4.6).

4.6 Western blot analysis

Western blotting was used to detect proteins of interest separated by SDS-PAGE.

4.6.1 Principle

Western blotting, also known as immunoblotting, is a method used to detect the presence of specific proteins after separation by SDS-PAGE. It consists of two main steps: the electrophoretic transfer of proteins from the polyacrylamide gel to a nitrocellulose membrane and the detection of the protein of interest using a specific antibody. The principles of antibody staining in Western blots are similar to those of immunofluorescence. However, the secondary antibody is commonly coupled to horseradish peroxidase (HRP), which allows protein visualization using

chemiluminescent detection methods. When the immunoblot is incubated with a chemiluminescent agent, the substrate is cleaved by HRP to generate a reaction product, which produces luminescence in proportion to the amount of protein. This light is then detected by a special camera that captures a digital image of the blot.

4.6.2 Protein transfer to nitrocellulose

The following protocol is described for the Mini Trans-Blot® Electrophoretic Transfer Cell from Bio-Rad. The resolving gel was soaked in cold transfer buffer (25 mM Tris, 190 mM glycine, 10% methanol), along with two pieces of Whatman filter paper, a nitrocellulose membrane, and two fiber pads. The transfer apparatus was assembled in the following order: fiber pad, Whatman filter paper, SDS gel, nitrocellulose membrane (pore size 0.2 μm), Whatman filter paper, and fiber pad. Air bubbles were removed, and the transfer was carried out at 100 V for 60 min in an immunoblot tank assembled according to the manufacturer's instructions.

Following transfer, the membrane was washed for 30 min in TBS-Tween (20 mM Tris-HCl, pH 7.5, 150 mM NaCl, 0.1% Tween) and subsequently stained with Ponceau S (0.1% in 5% acetic acid) in order to verify protein transfer and to aid with excision into lanes. Each lane was transferred into a separate well and stained with a particular antibody (see Section 3.4.2, **Table 13**).

4.6.3 Protein detection/immunostaining

Ponceau S was washed out with TBS-Tween for 30 min. Each strip of membrane was then incubated in 2 ml of blocking buffer (TBS-Tween containing 5% dry milk) for 1 h at RT in order to block unspecific antibody binding. The primary antibody was diluted in blocking buffer as described in **Table 13** (see Section 3.4.2) and added to the nitrocellulose membrane (1.5 ml) for overnight incubation at 4°C. The next day, the membrane was washed for 2 h with blocking buffer and then incubated for 2 h with the secondary antibody coupled to HRP diluted in blocking buffer (see Section 3.4.2, **Table 13**). The membrane was washed for 1 h with TBS-Tween.

In order to detect the antibody-labeled proteins, the membrane was incubated with 4 ml of

Supersignal® WestPico chemiluminescent substrate (kit solutions mixed 1:1) for 5 min. The immunoreactive bands were visualized using a Luminescent Image Analyser LAS-3000 dark box. The length of exposure time varied from 30 sec to 10 min, depending on the strength of the signal.

4.7 Data analysis and quantification

For quantification, cells were counted from the whole coverslip or a representative area of the coverslip. Statistical analyses were performed using Excel. The data were expressed as a mean ± standard deviation or as a total number per coverslip.

For pixel intensity quantifications, standard Leica confocal software was used to define regions of interest (ROIs), and the total fluorescence intensity for the appropriate channel was calculated for the summed optical sections/z-stacks. The total fluorescence was divided by the area of the ROIs to yield a pixel intensity per unit area. Background fluorescence was also measured and subtracted from the total fluorescence intensity.

Stable expression of a GFP-coupled construct of Rab1A in NRK cells allowed the identification of a novel domain of the IC, which associates with the centrosome and thus is designated as the pericentrosomal IC (pcIC) [7]. This domain is normally masked by the Golgi ribbon but can be identified as a distinct structure during cellular events that involve centrosome relocation, e.g., at the onset of mitosis [7]. Subsequent studies revealed that the pcIC receives cargo proteins from the ER and is resistant to treatment of cells with BFA, which releases COPI coats and results in complete Golgi disassembly [7]. Importantly, these studies have also demonstrated that protein transport to the PM still occurs in the presence of BFA, suggesting a role for the pcIC in Golgi-independent trafficking [7]. The increased overlap between the pcIC and the centrosome-associated ERC after BFA treatment suggested that the pcIC and ERC together form a stable pericentrosomal membrane system (PCMS) that functions as a way station during PM delivery of newly synthesized proteins bypassing the Golgi [7]. Thus, the pcIC may operate as an important sorting site in both Golgi-dependent and -independent trafficking to the cell surface [7]. Because of the known role of acidification in protein sorting, e.g., within the endosomal system and the TGN, it was of interest to investigate its importance in trafficking via the pcIC.

5.1 Effect of pH neutralization on BFA-induced redistribution of mannosidase II in interphasic cells

In these experiments, the trafficking of the medial Golgi enzyme mannosidase II (Man II) via the pcIC was investigated in NRK cells. Previous studies of interphasic cells showed that the pcIC contains a variable pool of Man II, indicating that this protein continuously cycles between the Golgi and the IC, using the pcIC as a way station [7]. Furthermore, BFA causes the redistribution of Man II from the Golgi to the ER via the pcIC, which persists in drug-treated cells [7]. Assuming that the pcIC is an acidic compartment, the disruption of its lumenal pH with acidification inhibitors would be expected to affect protein trafficking at the level of this organelle. Therefore, the following experiments addressed whether the BFA-induced redistribution of Man II is inhibited by various compounds that are known to result in the neutralization of acidic organelles.

Figure 8 shows the BFA-induced redistribution of Man II in the presence of the neutralizing agent ammonium chloride (NH_4Cl). Steady state cultures of GFP-Rab1A-expressing NRK cells

were pretreated for 3 h with NH_4Cl (10 mM), whereafter BFA (5 µg/ml) was added to the medium for 10 or 30 min in the continued presence of NH_4Cl. Long-term pretreatment with the acidification inhibitor was chosen due to the observed effect of neutralization on pcIC tubulation (data not shown). Control samples were treated for 10 or 30 min with BFA only. As shown in **Figure 8A** (control), already after 10 min of BFA treatment, the Golgi apparatus has fully disassembled, as indicated by the absence of Golgi-type Rab1A and Man II labeling, and Man II assumes an ER-like distribution. Consistent with previous results [7], the pcIC remains as a distinct Rab1A-containing structure in the presence of the drug. In contrast, pretreatment with NH_4Cl results in the accumulation of Man II in the pcIC, as indicated by the colocalization of Rab1A and Man II in the perinuclear area of cells treated with BFA for 10 min. This finding indicates that NH_4Cl at least partially inhibits the BFA-induced redistribution of Man II from the Golgi to the ER and that the protein becomes arrested in the pcIC. Notably, after 30 min treatment with BFA, the amount of Man II accumulating in the pcIC, as indicated by the red fluorescence signal, appears to be reduced compared to 10 min of drug treatment, suggesting that NH_4Cl does not completely block Man II redistribution, but rather causes a delay.

Quantification of the number of cells showing Man II accumulation in the pcIC, as indicated by its colocalization with Rab1A, in the above described experimental conditions is shown in **Figure 8B**. 10 min of BFA treatment (control) is sufficient to redistribute the bulk of Man II to the ER, and only very few cells show Man II-positive pcICs. However, after the 3 h NH_4Cl pretreatment, approximately 55% of the cells exposed to BFA for 10 min show Man II accumulation in the pcIC. By 30 min of BFA treatment, this value decreases to approximately 20%, with the majority of cells instead showing an ER-like distribution of Man II. The observed preferential accumulation of Man II in the pcIC at early time points after BFA addition strengthens the conclusion that NH_4Cl causes a delay in Man II redistribution to the ER.

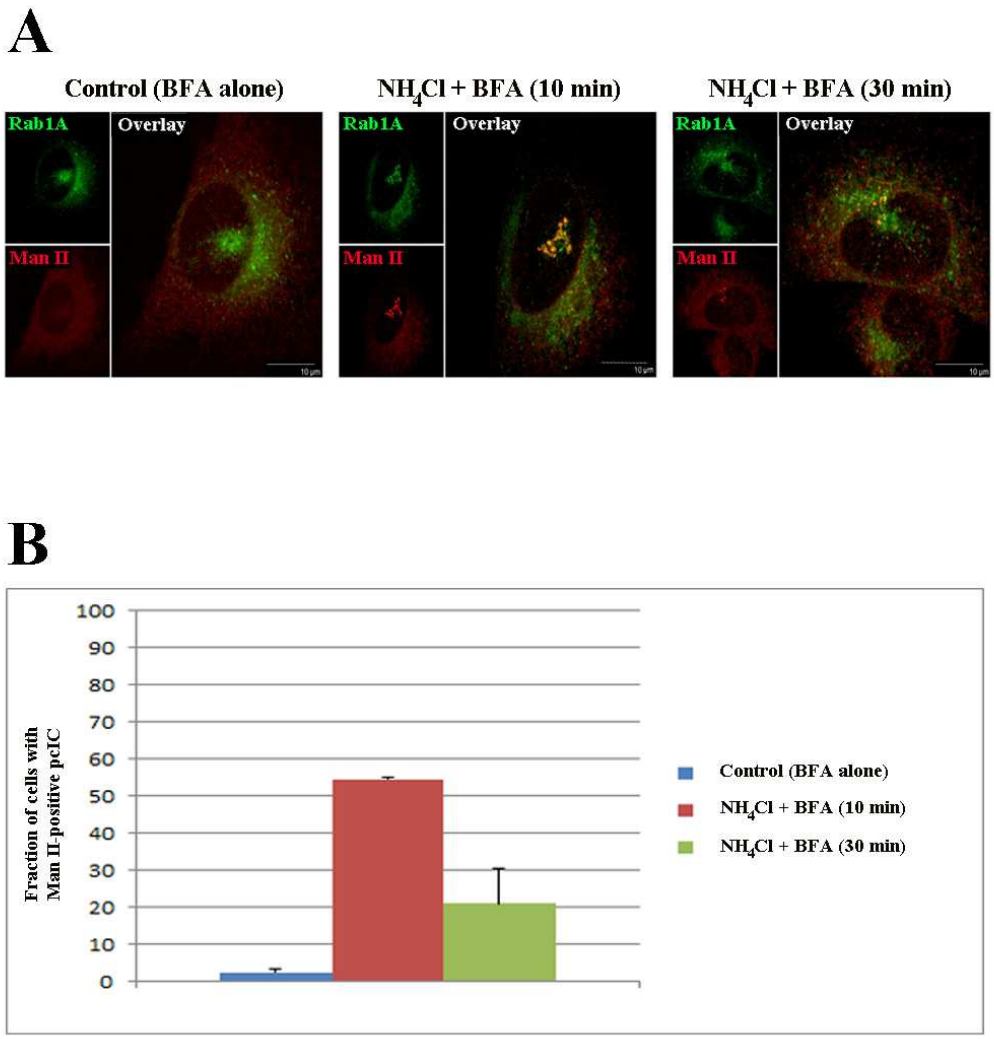

Figure 8. Effect of NH_4Cl on BFA-induced redistribution of Man II from Golgi to the ER. (A) NRK cells expressing GFP-Rab1A were treated for 10 or 30 min with BFA (5 µg/ml) after 3 h pretreatment with NH_4Cl (10 mM) and labeled with polyclonal anti-Man II. Rab1A is shown in green, Man II in red, and colocalization is indicated by the yellow color. Scalebars: 10 µm. (B) The percentage of cells showing colocalization of Man II with Rab1A in the pcIC was determined for each condition (n=100).

The cells exposed to the different experimental conditions (**Figure 8**) displayed considerable variability in the extent of Man II accumulation in the pcIC. Therefore, the pcIC pools of Man II were quantified more precisely to yield numerical values corresponding to the relative amounts of the protein. This allowed more accurate comparison of the different conditions, thus providing a better assessment of the effect of NH_4Cl on BFA-induced Man II redistribution. For each sample,

the pixel intensity of Man II fluorescence within the region of interest (ROI) defined by the Rab1A-positive pcIC was measured using standard Leica confocal software. **Figure 9A** illustrates the application of this method in the case of control cells (BFA alone, 10 min), showing the ROIs drawn around each separate pcIC defined by Rab1A. Subsequently, the pixel intensities of the selected ROIs were calculated by measuring the fluorescence intensity within the Man II channel (red) for each optical section. Since the size of the pcIC varies between different cells (and may also be affected by the different experimental conditions), the resulting total fluorescence signals were divided by the areas of the corresponding ROIs. The obtained values, representing the average pixel intensities per unit area, provide more accurate estimates of the pcIC pools of Man II under the different experimental conditions.

The relative amounts of Man II present in the pcIC at various times after BFA addition (0, 5, 10, 20, 30 min), measured by the above described method, are shown in **Figure 9B**. The control cells (exposed to BFA alone) and cells pretreated for 3 h with NH_4Cl prior to BFA addition are indicated by the blue and red curves, respectively. Under both conditions, the pixel intensity gradually decreases during the 30 min of BFA treatment, resulting in the general downward slopes of the two curves. This finding indicates that the amount of Man II in the pcIC diminishes in the course of the BFA treatment, as the protein in both cases evidently redistributes to the ER. Importantly, these results verify that NH_4Cl pretreatment of cells does not completely block the BFA-induced redistribution of Man II. It is noteworthy that the measured amounts of Man II in the pcIC prior to BFA addition are very similar for both the control and NH_4Cl-treated cells. This is in accordance with other results showing that long-term treatment with NH_4Cl does not have a measurable effect on the pcIC pool of Man II (data not shown). However, a significant difference between the control and NH_4Cl-pretreated cells is observed shortly after BFA addition, being most pronounced after 5 and 10 min of BFA treatment and corresponding to an approximately two-fold difference at the 10 min time point. The larger relative amount of Man II measured in the pcIC of cells pretreated with NH_4Cl clearly indicates that this compound interferes with the BFA-induced redistribution of the protein. By 30 min of BFA treatment, the pixel intensities determined for control and NH_4Cl-pretreated cells become more similar, which is consistent with the above described results indicating that NH_4Cl partly inhibits the redistribution of Man II to the ER. In control cells, the redistribution of Man II to the ER is nearly complete after 30 min of BFA treatment.

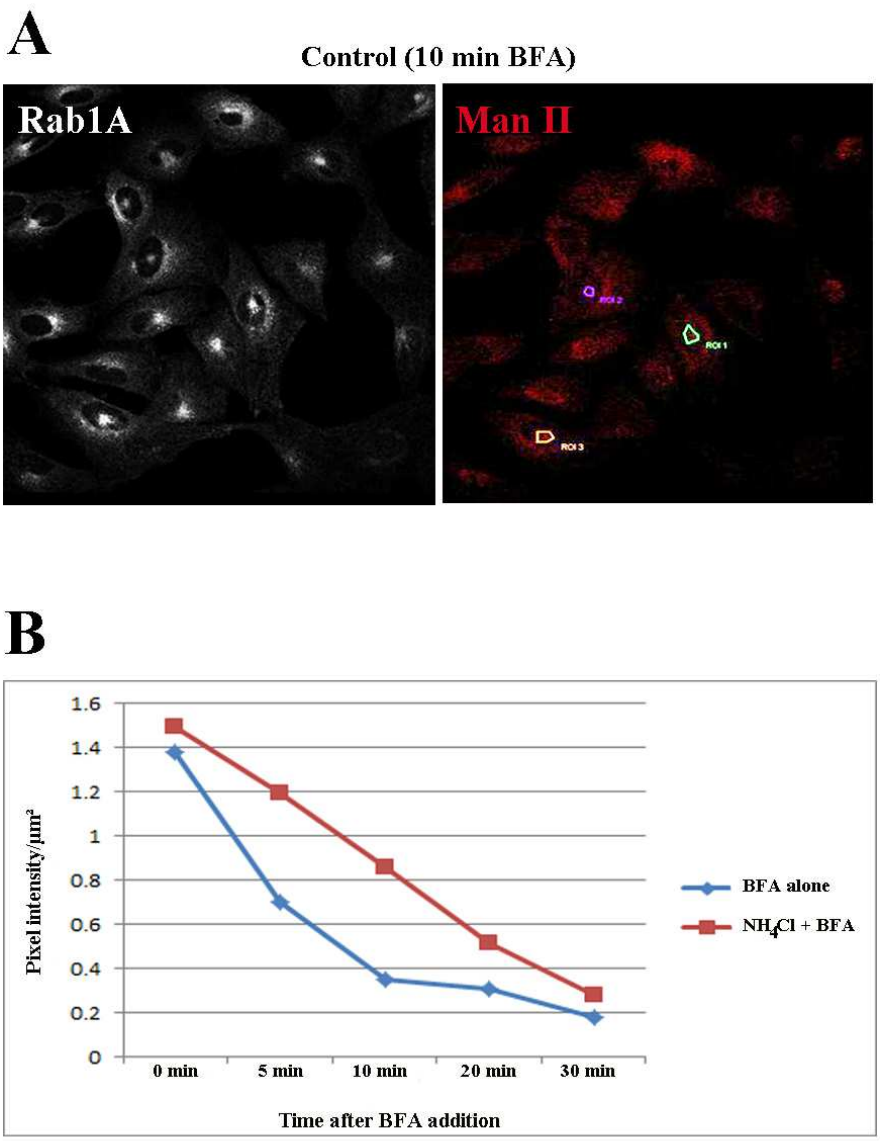

Figure 9. Determination of the relative amounts of Man II in the separate pcICs (ROIs) after BFA addition in the absence or presence of NH_4Cl. (A) NRK cells stably expressing GFP-Rab1A were incubated for 3 h in the absence or presence of NH_4Cl (10 mM) and subsequently treated with BFA (5 µg/ml) for 0, 5, 10, 20, and 30 min. The cells were fixed, stained with polyclonal anti-Man II, and examined by confocal microscopy. Pixel intensities were determined for each optical section (5-7 sections, 0.3-0.4 µm in thickness) by measuring the Man II-specific red fluorescence (right panel) in regions of interest (ROIs) defined by the separate Rab1A-positive pcICs at the cell center (left panel). The images show control cells treated for 10 min with BFA. (B) Average pixel intensities per unit area (n=20) were plotted for the indicated time points after BFA addition.

In conclusion, the above results strongly indicate that acidification facilitates the BFA-induced redistribution of Man II from Golgi apparatus to the ER. Interestingly, treatment of cells with NH_4Cl results in the accumulation of Man II in the pcIC, suggesting that neutralization of the

lumenal pH of this organelle interferes with the proper sorting of Man II to retrograde transport carriers. Notably, the inhibitory effect of NH_4Cl is only temporary, since after 30 min of BFA treatment, the accumulation of Man II in the pcIC, as compared to control cells, is considerably less pronounced than after short (5 to 10 min) treatments with the drug. Moreover, after 30 min of incubation with BFA, the number of cells showing Man II accumulation in the pcIC is considerably reduced (**Figure 8**).

5.2 Effect of pH neutralization on redistribution of Man II during mitosis

As described above (Section 1.5), the Golgi undergoes complete disassembly during mitosis. The resulting Golgi haze, which mediates the partitioning of the organelle into the forming daughter cells, corresponds either to numerous free vesicles or Golgi components fused with the ER [40,58]. Recent live-cell imaging of IC dynamics in NRK cells expressing GFP-Rab1A have revealed that the mitotic IC maintains many of its interphasic features, including its association with the centrosome (M. Marie, H. Dale, N. Kouprina, J. Saraste, manuscript in preparation). Notably, the pcIC divides at the onset of mitosis and forms large clusters that at metaphase accumulate around the spindle poles. The preservation of this compartment during mitosis has raised the possibility that the tubulovesicular IC clusters serve as way stations in the redistribution of Golgi components into the mitotic Golgi haze. This alternative mechanism of Golgi partitioning, implicating the IC in mitotic redistribution of Golgi components, contrasts with the two previous models described in Section 1.5.2.

Interestingly, the above described experiments (Section 5.1) have provided evidence that while NH_4Cl treatment of interphasic cells only partially blocks the redistribution Man II to the ER, it efficiently inhibits the relocation of the protein in mitotic cells, i.e., the formation of the mitotic Golgi haze. To verify this observation, steady state cultures of GFP-Rab1A-expressing NRK cells were treated for 60 min with NH_4Cl prior to fixation, and cells at metaphase were identified by DAPI staining. As shown in **Figure 10A**, both control metaphasic cells, as well as cells treated with NH_4Cl, contain the punctate IC clusters that typically associate with the spindle poles, consistent with earlier results (M. Marie, H. Dale, N. Kouprina, J. Saraste, manuscript in preparation). However, the localization of Man II in metaphasic cells revealed that while the labeling of the untreated cells is predominantly diffuse, corresponding to the mitotic Golgi haze,

the NH_4Cl-treated cells display a significantly more punctate pattern. Furthermore, extensive colocalization of Man II and Rab1A was observed in the spindle region of the drug-treated cells. In conclusion, these results show that NH_4Cl blocks the redistribution of Man II into the mitotic Golgi haze and results in its accumulation in Rab1A-positive metaphasic IC clusters. Thus, they are in accordance with the possibility that the latter serve as way stations during the redistribution of Golgi components.

Due to the variability in Man II labeling, quantification was performed to determine more precisely the localization of Man II in metaphasic cells exposed to the different experimental conditions (**Figure 10B**). The distributions of the protein in untreated cells, determined for both the parental and GFP-Rab1A-expressing NRK cells (control), were very similar. Both cell types show nearly equal expression of the diffuse and punctate patterns, with a slight predominance of the "haze" phenotype (~55% versus 45% in the case of parental NRK cells). Notably, NH_4Cl treatment results in a dramatic decrease in the number of cells exhibiting the "haze" phenotype (less than 5% for both cell types) and leads to the appearance of abnormally large structures (in more than 45% of cells), containing both GFP-Rab1A and Man II. Finally, NH_4Cl washout results in considerable reduction of the number of cells expressing the large structures with a corresponding increase in the fraction of cells displaying the typical Golgi haze pattern. Importantly, similar results were obtained for the GFP-Rab1A-expressing cells and the parental NRK cells, in which endogenous Rab1 was localized using affinity-purified antibodies. Overall, the quantification of Man II localization in metaphasic cells verified that NH_4Cl treatment blocks the redistribution of the protein into the mitotic haze, resulting in its efficient arrest in the Rab1A-containing mitotic IC clusters. In addition, these results are in agreement with previous studies [45] in showing that the effect of this compound on protein sorting and/or transport is reversible.

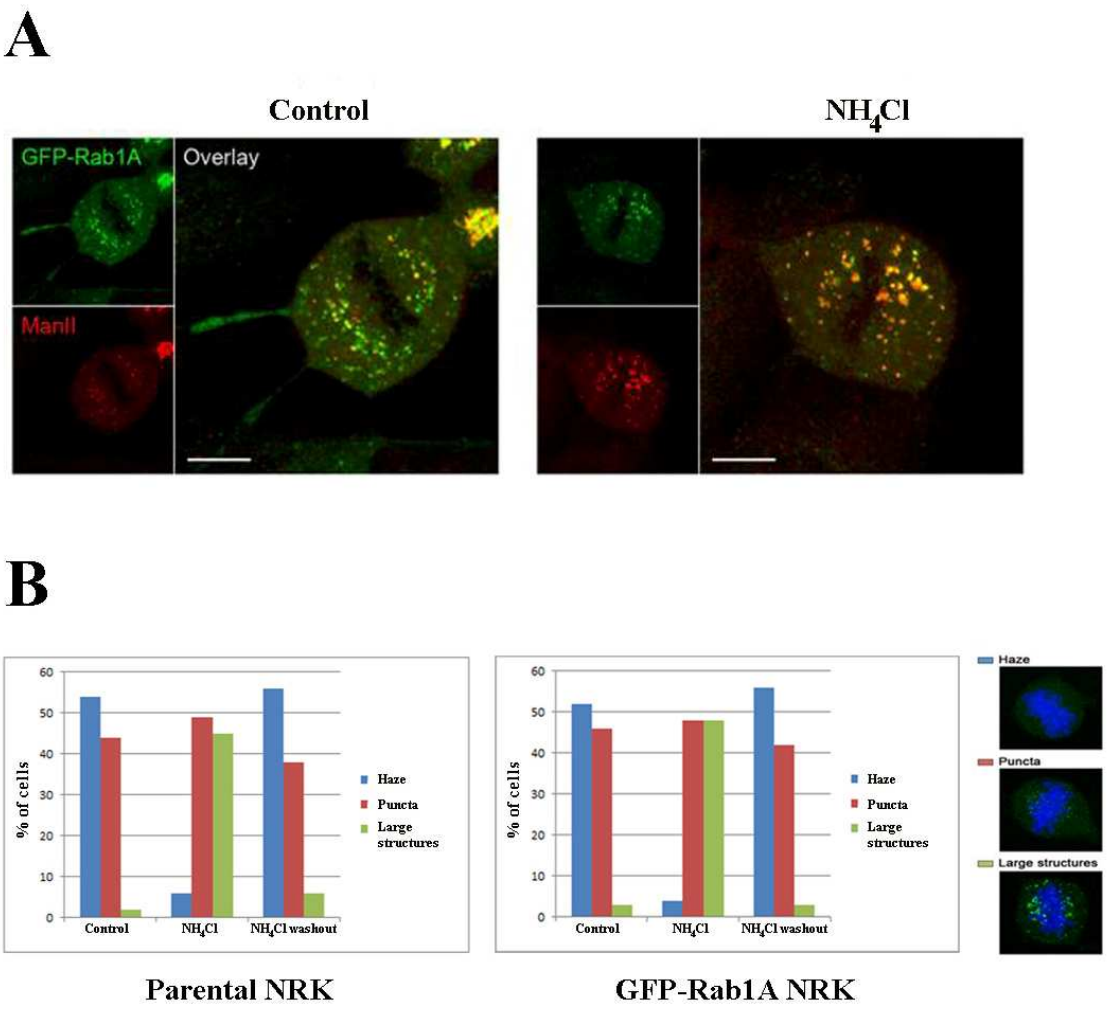

Figure 10. Effect of NH_4Cl on mitotic redistribution of Man II. (A) Steady state cultures of NRK cells expressing GFP-Rab1A were treated for 60 min with NH_4Cl (10 mM) and stained with polyclonal antibodies against Man II. Mitotic cells at metaphase were identified by DAPI labeling. Rab1A and Man II are shown in green and red, respectively, and colocalization is indicated by the yellow color. Scalebars: 10 µm. (B) Quantification of Man II localization in parental and GFP-Rab1A-expressing NRK cells. The cultures were treated for 60 min with 10 mM NH_4Cl, and the washout was performed by first rinsing the cells extensively with drug-free culture medium and then incubating them in the same medium for an additional 2 h. Man II labeling of metaphasic cells (n=200 for each condition) was scored as haze, puncta, or large structures according to the patterns shown in the images on the right. DNA staining (DAPI) is shown in blue.

The effect of other acidification inhibitors on the mitotic redistribution of Man II was also evaluated. For this purpose, steady state cultures of GFP-Rab1A-expressing NRK cells were treated for 2 h with 0.5 µM bafilomycin A1 (**Figure 11A**) or 100 µM chloroquine (**Figure 11B**). Notably, incubation of cells in the presence of these inhibitors resulted in the accumulation of

Man II in large Rab1A-positive membrane clusters in metaphasic cells, similar to the structures seen in NH_4Cl-treated cells. Thus, pH neutralization with different compounds appears to result in a general arrest of Man II in the mitotic IC clusters, blocking its dispersal into the Golgi haze. Importantly, the similar results obtained with the different inhibitors indicate that the efficient transport arrest exerted by NH_4Cl in mitotic cells is not due to indirect effect(s) of the drug. In summary, the collective results obtained using confocal microscopy are in accordance with the conclusion that lumenal acidification of the IC plays a significant role during the relocation of Man II during mitosis. Generally, the IC clusters could act as way stations during the redistribution of Golgi proteins, providing a basis for an alternative model of mitotic Golgi partitioning.

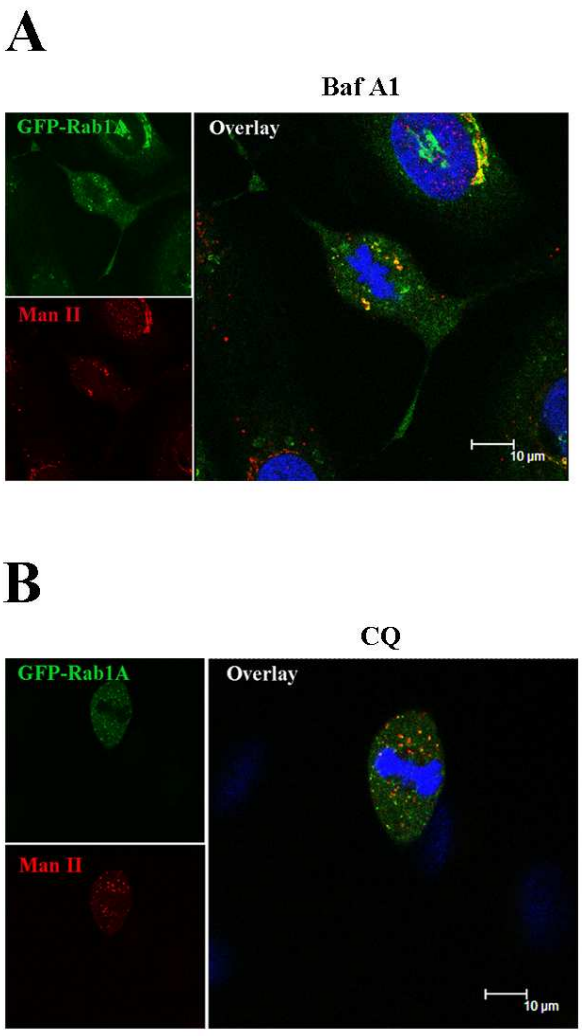

Figure 11. Effect of bafilomycin A1 and chloroquine on the redistribution of Man II during mitosis. NRK cells expressing GFP-Rab1A were treated for 2 h either with (A) 0.5 µM bafilomycin A1 (Baf A1) or (B) 100 µM

chloroquine (CQ) and stained with monoclonal antibodies against Man II. Rab1A and Man II are shown in green and red, respectively, and colocalization is indicated by the yellow color. DNA staining (DAPI) is shown in blue. Scalebars: 10 μm.

To validate the confocal results showing increased colocalization of Man II with Rab1A after the treatment of mitotic cells with acidification inhibitors, cell fractionation of both control and NH_4Cl-treated cells was performed. These pilot experiments involved steady state cultures of parental NRK cells and the isolation of mitotic cells by mechanical shake-off. Unfortunately, since cell synchronization was not employed, only small amounts of material were recovered in the fractions collected from the glycerol gradients (see Section 4.4.3), and as a consequence, the proteins of interest could not be detected by Western blotting.

5.3 Effect of brefeldin A on redistribution of Man II during mitosis

To complement the above results obtained using acidification inhibitors, the effect of brefeldin A (BFA) on the mitotic redistribution of Man II was examined in subsequent experiments. These studies were partly based on the surprising observation of Nizak and coworkers [72], showing that the addition of BFA during the prometaphase-metaphase transition (via microinjection of individual living mitotic cells) results in the accumulation of Golgi enzymes in BFA-resistant membranes of unknown nature. By contrast, microinjection of the drug during anaphase, telophase, or cytokinesis lead to the expected redistribution of the enzymes to the ER, as similarly observed during interphase [72]. Since recent studies of interphasic cells revealed that the IC is a BFA-resistant organelle [7], it was of interest to investigate whether the BFA-resistant, Golgi enzyme-containing structures observed by Nizak and coworkers [72] correspond to the Rab1A-positive IC clusters that persist and maintain their BFA-insensitivity during mitosis.

To study the mitotic effects of BFA and the previously described acidification inhibitors, several pilot experiments were carried out in order to design an assay that would facilitate the morphological investigation of large numbers of cells undergoing early steps of mitosis. Optimally, such a method should generate a wave of cells progressing from prophase (or prometaphase) to metaphase in a relatively synchronized fashion, thus providing a kinetic assay (i.e., a short “time window”) that allows detailed evaluation of the effects of inhibitors on mitotic relocation of Golgi components. As one attempt to devise such an assay, steady state cultures of

NRK cells grown on glass coverslips were subjected to careful, but sufficiently extensive flushing with ice-cold medium, which was expected to selectively remove the less adherent mitotic cells (metaphase, anaphase, and telophase), but not detach the more tightly substrate-bound cells (interphase, prophase, prometaphase, and cytokinesis). Subsequently, the cells were returned to warm growth medium and fixed at the indicated time points after incubation at 37^{o}C (0, 15, 30, and 60 min). As shown in **Figure 12**, the flushing of the cultures resulted in efficient detachment of practically all metaphasic cells, as determined by DAPI staining of cultures fixed at the 0 min time point, as well as most cells undergoing anaphase and telophase (data not shown). However, the number of metaphasic cells rapidly increased during the post-flush incubation, reaching a plateau (~200 metaphasic cells per coverslip) after about 30 min at 37^{o}C (**Figure 12**, control).

Since the flush assay appeared to fulfill the above described methodological requirements, it was first applied to investigate the possible effects of inhibitors on mitotic progression of NRK cells. Accordingly, BFA (5 µg/ml) and NH_4Cl (10 mM) were added to the cells immediately after the removal of mitotic cells by flushing, and samples were recovered and fixed after different times of incubation at 37^{o}C in the drug-containing medium. The data obtained with untreated cells (**Figure 12**, control) indicated that the metaphasic cells that eventually appear in the presence of BFA or NH_4Cl would have been exposed to the inhibitors only during a short time period, as they progressed through the early steps of mitosis. Importantly, determination of the number of metaphasic cells by DAPI staining revealed that neither of the drugs exerts a block on early mitotic progression. On the contrary, both the BFA- and NH_4Cl-treated cultures generated a new wave of metaphasic cells very rapidly. In both cases, the number of metaphasic cells reached a maximum already after 15 min (**Figure 12**, BFA and NH_4Cl), i.e., with kinetics that are considerably faster than observed for the control cells. However, although these preliminary results indicate that the drugs may affect the kinetics of mitotic progression, further studies are required to verify this conclusion.

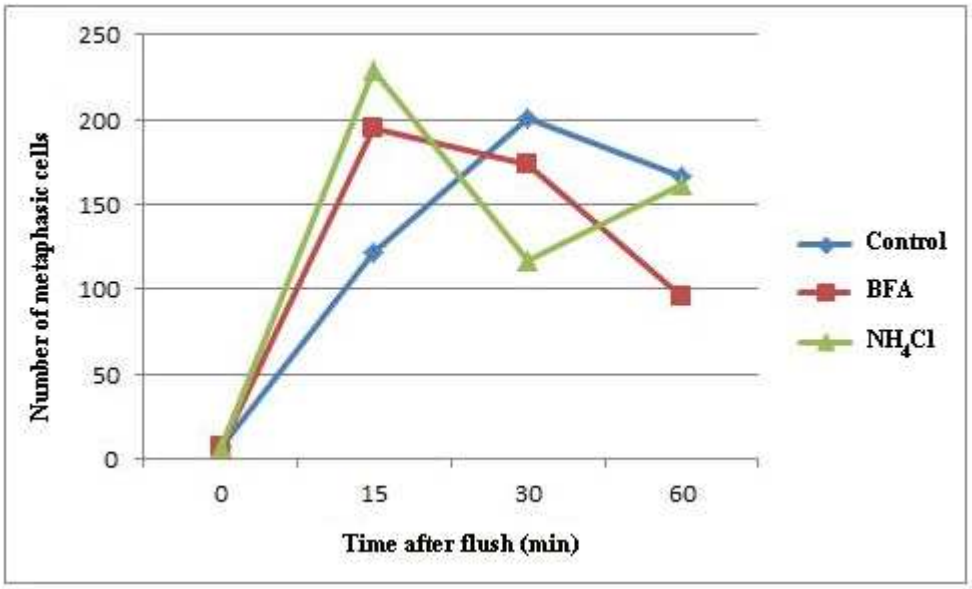

Figure 12. Application of the flush assay to study the effects of BFA and NH_4Cl on mitotic progression of NRK cells. In order to generate a wave of cells progressing through the early steps of mitosis towards metaphase, parental NRK cells grown on glass coverslips were subjected to extensive flushing with ice-cold medium to release the less adherent mitotic cells. The cultures were then incubated for the indicated times (0, 15, 30, or 60 min) at 37°C in normal growth medium (control, blue), or medium supplemented with BFA (5 µg/ml, red) or NH_4Cl (10 mM, green). The number of metaphasic cells per coverslip, both remaining bound to the cell monolayers after the flushing (0 time point) and appearing during the different incubations, was determined for each time point after fixation and DAPI staining.

Nevertheless, since the flush assay provided a valuable means to generate a relatively synchronized wave of cells progressing towards metaphase, it could be readily applied to study the effect of BFA on the mitotic redistribution of Man II in GFP-Rab1A-expressing NRK cells. Previous results (see **Figure 10A**) have indicated that while the majority of control NRK cells at metaphase display a diffuse Man II pattern corresponding to the mitotic Golgi haze, many cells also contain variable amounts of large Man II-containing structures that typically localize to the vicinity of the spindle poles**.** Notably, these puncta are also positive for Rab1A, indicating that they correspond to the mitotic IC clusters (shown in **Figure 13A**). By contrast, the metaphasic cells appearing in BFA-treated cultures display much more extensive accumulation of Man II in these punctate, Rab1A-containing structures. Because BFA does not block mitotic progression and the flushing efficiently removes the metaphasic cells (**Figure 12**), this dramatic effect of the drug is most likely exerted at an earlier stage of mitosis, i.e,. as the cells progress towards metaphase. This observation supports the conclusion that the inability of BFA to induce Man II

relocation to the ER during late prometaphase and metaphase [72], in contrast to other stages of the cell cycle, is due to the temporary presence of this Golgi enzyme in the BFA-resistant IC elements.

The intracellular distribution of the COPI coats in the absence or presence of BFA is also illustrated in **Figure 13B**. In untreated control cells (fixed 10 min after the flush), the COPI coats predominantly associate with the IC clusters at the spindle poles of the nascent metaphasic cells, showing that mitotic progression does not affect their binding to membranes. By contrast, the presence of BFA in the medium during the 10 min post-flush period results in the release of the coats and their redistribution to the cytosol, verifying the efficacy of the drug under these conditions.

Finally, quantification of the Man II labeling patterns in control and BFA-treated metaphasic cells subjected to the flush procedure was carried out (**Figure 13C)**, employing the previously described criteria (see **Figure 10**). To obtain preparations enriched in metaphasic cells, the mitotic cells appearing during the 10 min post-flush period were released (by shake-off) and re-attached to poly-L-lysine-coated coverslips. As an additional control, part of the cultures were treated for 30 min with BFA preceding the flush and fixed after an additional 10 min post-flush incubation in the presence of the drug (pre-BFA). The untreated metaphasic cells stained with anti-Man II consist of two main populations, displaying either the punctate or haze patterns (**Figure 13C**, control). Interestingly, in these samples, the fraction of cells containing punctate structures (~65%) is significantly higher than in the steady state cultures (**Figure 10B**, ~45%), suggesting that this pattern may be typical for early metaphasic cells. The fraction of cells displaying the haze pattern (less than 10%) is greatly reduced in metaphasic cells appearing during the 10 min BFA treatment. There is a corresponding increase in the number of cells containing large, Man II-positive structures that are typically not seen in the untreated cells. About 60% of the drug-treated metaphasic cells display this pattern (**Figure 13C**, 10 min BFA). Since Man II is efficiently relocated to the widespread ER network when pre-mitotic cells are treated with BFA, virtually all cells exposed to the drug prior to the flush exhibit a hazy pattern (**Figure 13C**, pre-BFA), which is indistinguishable from the Golgi haze of the untreated cells.

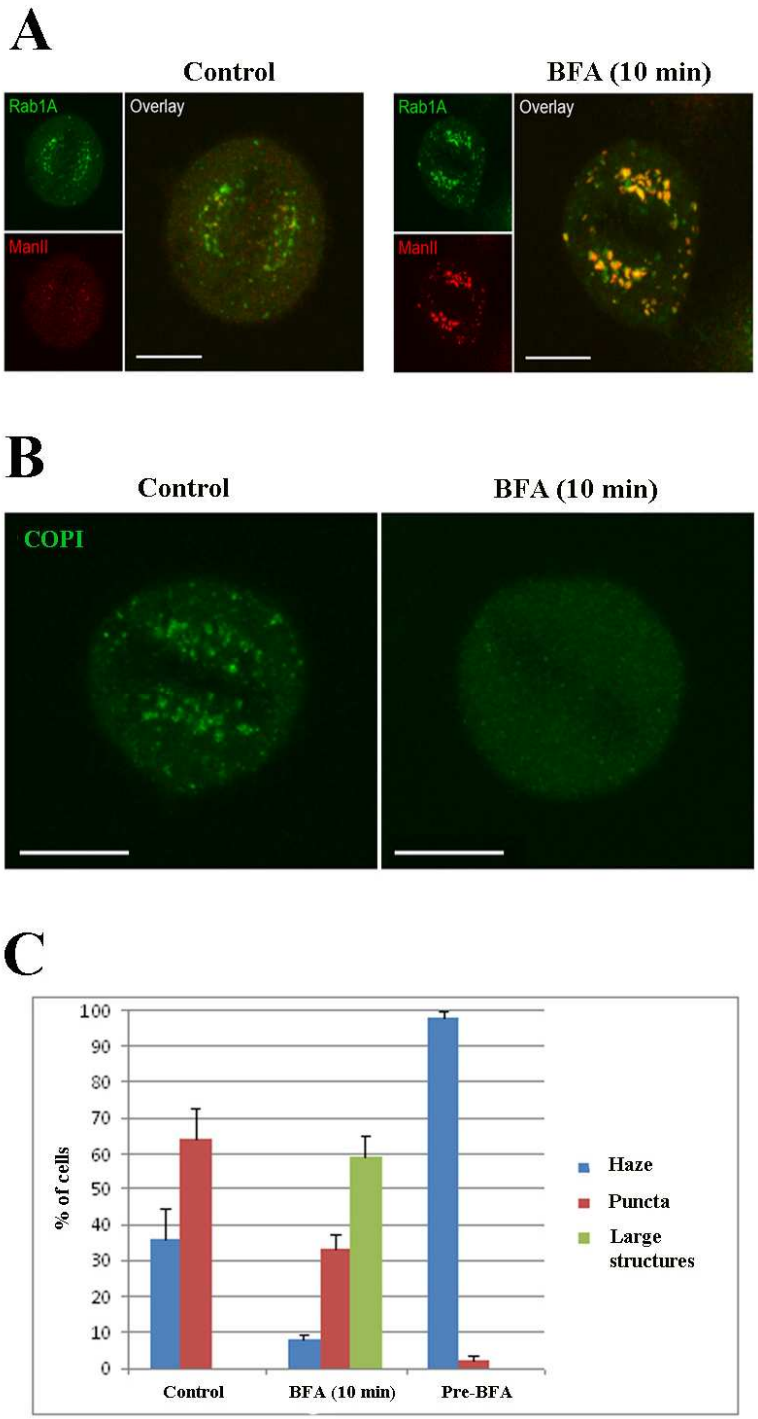

Figure 13. Application of the flush assay to study the effects of BFA in metaphasic cells. Following flushing, the parental (C) or GFP-Rab1A-expressing (A and B) cells were incubated for 10 min in the presence or absence of BFA. Part of the BFA-treated cultures were exposed to drug already 30 min prior to the flush (C, pre-BFA). Metaphasic cells reappearing after the removal were identified by DAPI staining. (A) Localization of Man II. Colocalization of Rab1A (green) and Man II (red) is indicated by the yellow color. (B) Localization of COPI coats using antibodies against β-COP. Scalebars: 10 µm. (C) Quantification of Man II patterns in metaphasic cells (see also Figure 10; n=100).

In conclusion, the above results provide strong evidence in favor of the idea that the IC functions as a way station during the redistribution of Golgi components, playing an important role in the formation of the mitotic Golgi haze. It is also noteworthy that the block exerted by BFA on the mitotic relocation of Man II is similar to the inhibitory effects of the acidification inhibitors (see Section 5.2).

5.4 Effect of low temperature on Man II localization during mitosis

A disadvantage of expensive drugs like BFA is that they cannot be readily employed in experiments that require mass preparations of unsynchronized mitotic cells (e.g., cell fractionation and immunoelectron microscopy). Therefore, to find additional conditions that affect the dynamics of Golgi proteins in dividing cells, the localization of Man II was studied in cells exposed to low temperature (15°C). These experiments were based on previous studies showing that incubation at 15°C alters the localization of peripheral Golgi proteins (e.g., giantin) in metaphasic cells [55]; however, these studies did not address the effect of low temperature on the mitotic distribution of integral membrane proteins, such as Man II. To investigate the effect of 15°C incubation on the localization of this Golgi enzyme, mitotic NRK cells expressing GFP-Rab1A were released by mechanical shake-off and bound to poly-L-lysine-coated coverslips. Subsequently, the cells were placed in a 15°C water bath and incubated for 15 or 30 min in pre-cooled medium supplemented with 20 mM HEPES (pH 7.2). Interestingly, after only a 15 min incubation of cells at the low temperature, considerable amounts of Man II relocate to punctate structures at the spindle poles, which partly colocalize with the Rab1A-positive IC clusters (**Figure 14B**, compare with **Figure 14A** showing control cells). This effect is also seen in cells incubated for 30 min at 15°C (**Figure 14C**). This finding suggests that the low temperature treatment results in the accumulation of Man II in the IC elements by preventing its normal dispersal into the vesicular Golgi haze, sharing similarity with the effects exerted by BFA and acidification inhibitors (see Sections 5.2 and 5.3). However, it is also possible that low temperature incubation blocks a specific step – for example, a membrane fusion event – that is required for mitotic Golgi disassembly.

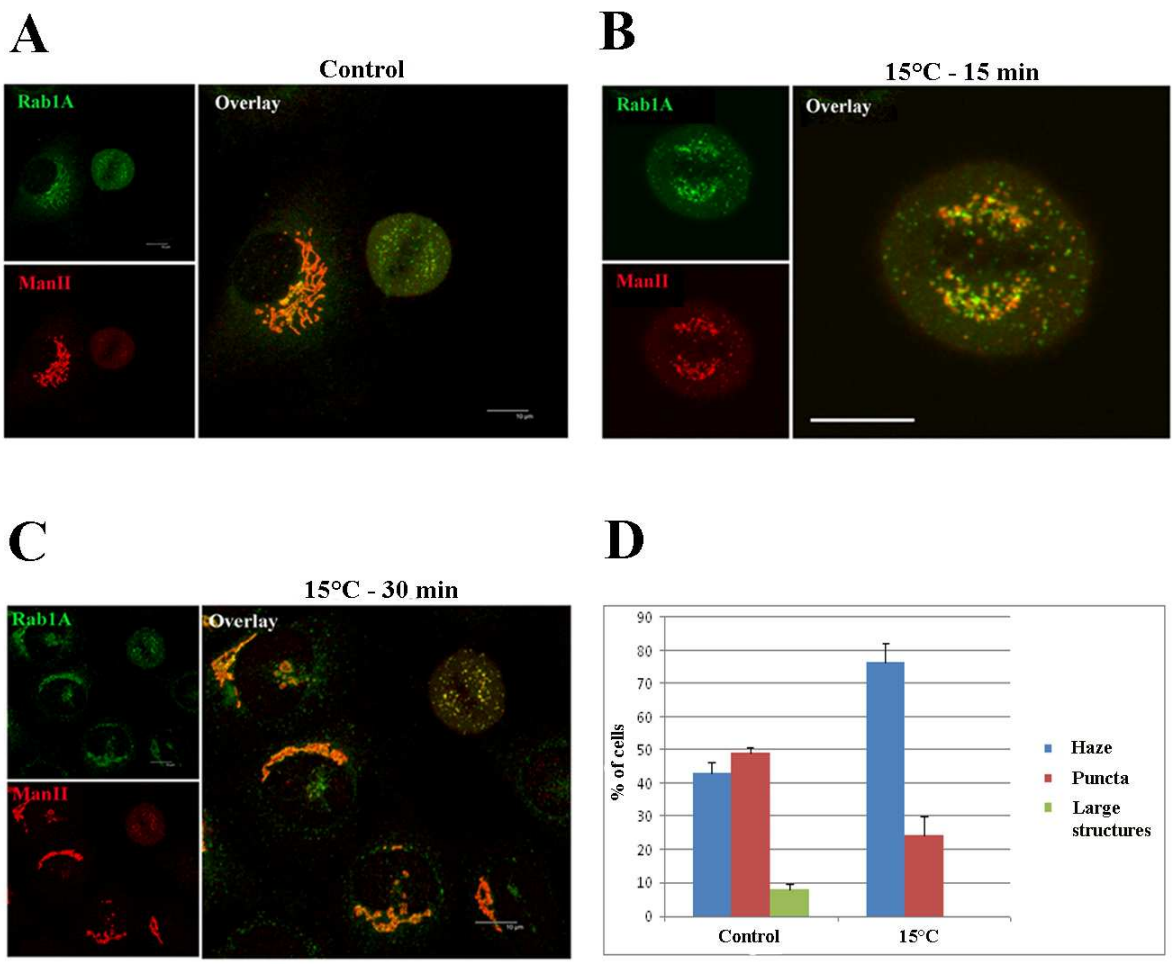

Figure 14. The effect of 15°C incubation on Man II redistribution during mitosis. Mitotic NRK GFP-Rab1A cells were collected by shake-off and bound to glass coverslips. Subsequently, the cells were incubated for 15 min (B) or 30 min (C) at 15°C, fixed, and stained with polyclonal antibodies against Man II. A control metaphasic cell, identified by DAPI staining, is shown in (A). Rab1A is shown in green, Man II in red, and colocalization is indicated by the yellow color. Scalebars: 10 µm. (D) Quantification of the distribution patterns of Man II (see **Figure 10B**) in parental NRK cells incubated for 30 min at 15°C (n=100). Following the low temperature treatment, the control cells were further incubated for 30 min at 37°C.

The effect of 15°C incubation on the distribution of Man II in metaphasic cells was quantified, as previously described for **Figure 10B**. Parental NRK cells were first incubated for 30 min in a 15°C water bath in pre-cooled medium supplemented with 20 mM HEPES (pH 7.2). A shake-off was performed to obtain samples enriched in mitotic cells, which were then attached to poly-L-lysine-coated coverslips and subsequently fixed. Control samples were prepared by returning the low temperature-treated cultured cells to 37°C for 30 min and then collecting the mitotic cells by mechanical shake-off. Interestingly, the quantification indicated that the Man II distribution

patterns seen in individual cells (**Figures 14A-C**) may not adequately describe the effect(s) of the 15°C incubation. Namely, rather than resulting in the general accumulation of Man II in punctate structures in metaphasic cells, the low temperature incubation appeared to considerably increase the fraction of cells displaying the haze phenotype (nearly 80%). In fact, following the 15°C treatment, the number of cells showing punctate patterns (~25%) was reduced by approximately two-fold as compared to the control cells (~50%) (**Figure 14D**). Furthermore, the cells incubated at 15°C did not exhibit the abnormally large Rab1A- and Man II-positive clusters that were encountered in a minority (~10%) of the control cells in this experiment (**Figure 14D**). These discrepant results may be due to unprecedented effects of different preparation steps on the mitotic cells and make it difficult to draw reliable conclusions concerning the true effects of the 15°C incubation (see Section 6.3).

Cell fractionation provides an alternative method to compare the localizations of Rab1 and Man II in mitotic cells exposed to the different experimental conditions, e.g., incubation at low temperature or in the presence of NH_4Cl. In the pilot experiment described below, the unsynchronized parental NRK cells were grown in large culture flasks, collected by shake-off, and incubated for 30 min at 15°C. The corresponding control cells (37°C) were fractionated immediately after the shake-off. Post-chromosomal supernatants were prepared by differential centrifugation and subjected to ultracentrifugation in Opti-Prep™ velocity gradients (see Section 4.4.2). After collection of the gradient fractions, membranes were concentrated by ultracentrifugation, and the final pellets were analyzed by SDS-PAGE and Western blotting (see Sections 4.5 and 4.6) using antibodies against Rab1, p58, and Man II.

The results are shown for the control and 15°C-treated cells in **Figures 15A** and **B**, respectively. Unfortunately, due to the small amounts of material recovered in the control gradient fractions, the antibodies against Man II and Rab1 resulted in only weak bands even after long exposure times. However, analysis of the 15°C-treated cells showed the enrichment and colocalization of Man II and Rab1 in fractions 3 and 4 at the top of the gradient. Interestingly, the enrichment of both Rab1 and p58 in slowly-sedimenting IC elements (fractions 3 and 4) and the additional presence of p58 in fast-sedimenting ER structures (fractions 6-8) are in accordance with previous studies of interphasic PC12 cells [71]. However, since p58 is relocated to the ER during mitosis (M. Marie, H. Dale, N. Kouprina, J. Saraste, manuscript in preparation), the finding of a major pool of the protein in the IC fractions is somewhat unexpected.

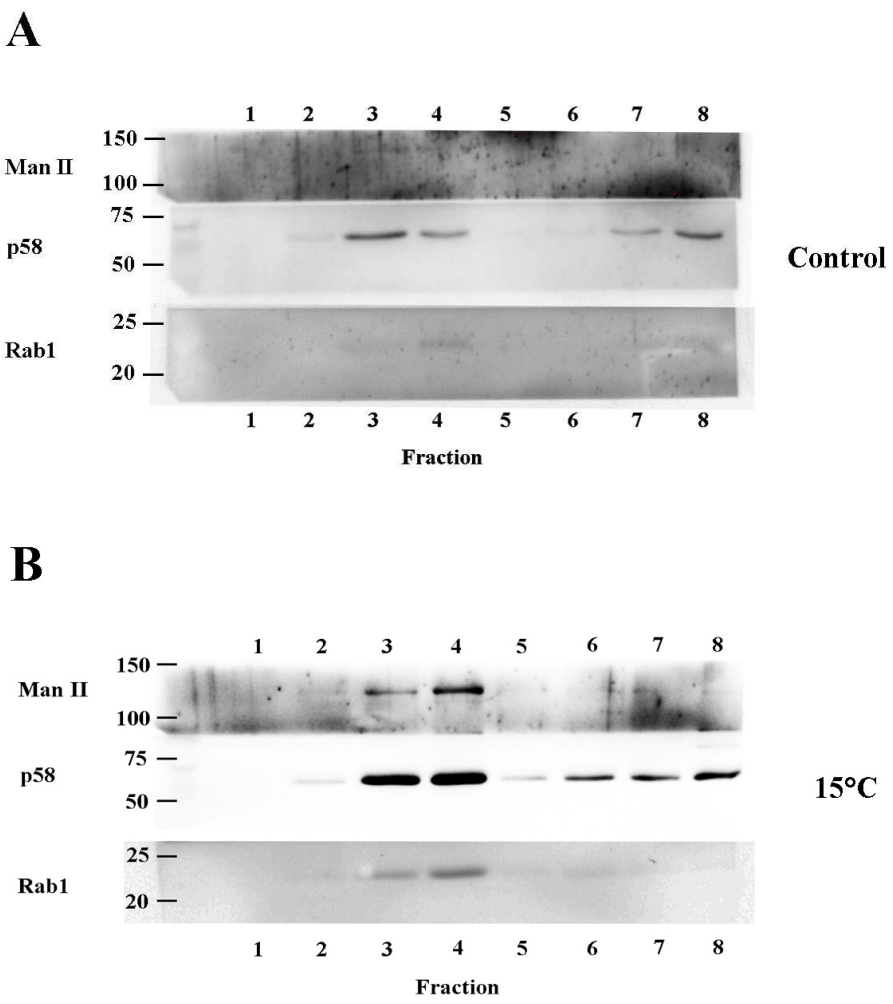

Figure 15. Application of velocity gradient sedimentation to study the effect of 15°C incubation on the localization of Man II in mitotic cells. Mitotic shake-offs of parental NRK cells were fractionated directly (A, control) or after 30 min incubation at 15°C (B) Post-chromosomal supernatants were prepared and subjected to velocity sedimentation in 5-25% iodixanol (Opti-Prep™) gradients. The gradient fractions (1-8) were analyzed by SDS-PAGE and Western blotting using antibodies against Man II, p58, and Rab1. The detected immunoreactive bands have expected molecular weights: Man II (~124 kDa), p58 (~58 kDa), and Rab1 (~22 kDa).

Although one explanation is that in mitotic cells, p58 is localized to a particular ER domain, whose sedimentation properties are similar to those of the tubulovesicular IC elements, another possibility is that the mitotic preparation(s) in this experiment were contaminated by interphasic cells. These preliminary and presently inconclusive findings are discussed further in Section 6.3.

6 Discussion

The studies presented in this thesis address the complex pathways and mechanisms of bidirectional membrane traffic at the ER-Golgi boundary, with particular emphasis on the role of the IC in these processes. Importantly, the results provide evidence that the IC is involved in the partitioning of the Golgi apparatus during mitosis, introducing a novel mechanism for Golgi inheritance that contrasts with the previously presented models. Furthermore, they indicate that the function of the IC in molecular sorting and trafficking throughout the cell cycle depends on its lumenal acidification, i.e., that the IC is a low pH organelle.

6.1 Role of the IC in mitotic Golgi partitioning

Strikingly, recent studies have revealed that the IC is an autonomous organelle, which persists and maintains its properties throughout the cell cycle, in particular, its close association with the centrosome (M. Marie, H. Dale, N. Kouprina, J. Saraste, manuscript in preparation). Live-cell imaging of IC dynamics in NRK cells stably expressing GFP-Rab1A showed that at the onset of mitosis (G2/M transition), the pericentrosomal IC (pcIC) moves away from the Golgi region and divides into two identical structures at prophase, in parallel with the separation of the duplicated centrosomes. The daughter pcICs maintain their association with the centrosomes, forming extensive membrane clusters at the spindle poles by metaphase. Since the IC plays an important role in Golgi biogenesis and maintenance during interphase, its preservation during cell division raises the possibility that the IC clusters are also involved in mitotic Golgi disassembly, functioning as way stations while the components of this organelle redistribute to form the Golgi haze. This new model of Golgi partitioning, implicating the IC in mitotic Golgi breakdown, is schematically illustrated in **Figure 16** (see legend for further details).

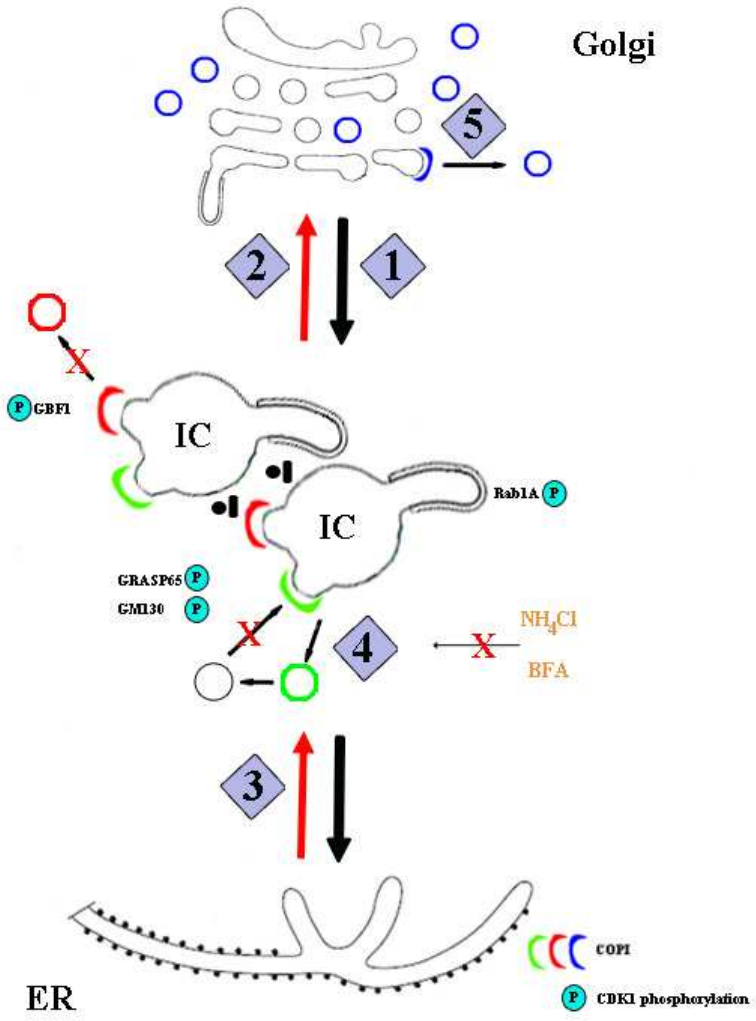

Figure 16. Role of the IC in mitotic Golgi partitioning. The onset of mitosis is marked by the separation of the centrosome and the associated pcIC from the Golgi ribbon (**Step 1**). Subsequent activation of cyclin B-CDK1 leads to phosphorylation of several targets at the pcIC, including Rab1A and GBF1. The phosphorylation of Rab1A inhibits tubular trafficking to the Golgi (possibly by affecting its association with a motor protein), whereas phosphorylation of GBF1 releases ARF1 from membranes. Since COPI coats remain membrane-bound, the modification of GBF1 could selectively release a particular COPI isotype (red coats) mediating IC-to-Golgi trafficking, thus blocking the budding or fusion (not shown) of the corresponding COPI vesicles. Accordingly, both COPI- and Rab1A-dependent IC-to-Golgi traffic could be disrupted by CDK1-mediated phosphorylation events (**Step 2**). In addition, ER exit is blocked due to the modification of COPII coats (**Step 3**). Inhibition of steps 2 and 3 results in the accumulation of recycling Golgi enzymes in the mitotic IC clusters ("punctate" Man II pattern), followed by their dispersal into the Golgi haze ("diffuse" Man II pattern) via ongoing formation of IC-derived COPI vesicles (green coats; **Step 4**). The fusion of these vesicles is blocked by CDK1-dependent phosphorylation of the tethering factors GRASP65 and GM130. Alternatively (or in addition), the formation of the Golgi haze could take place via direct COPI-mediated vesiculation of the organelle (blue coats; **Step 5**). This model assumes the operation of three different types of COPI vesicles (shown in red, green, and blue) in bidirectional trafficking in the early secretory pathway. The proposed inhibitory mechanisms for NH_4Cl and BFA are also depicted in this model, which

was prepared by the author.

A key feature of this model is the persistent association of the pcIC with the centrosomes during mitosis. This previously unrecognized connection is of importance, since centrosomes represent the site of activation of the mitotic kinases cyclin B-CDK1 and PLK1 [73,74], which regulate the events leading to mitotic Golgi reorganization and fragmentation [61,63,75]. As described in Section 1.5.1, Golgi ribbon unlinking and cisternal unstacking involve phosphorylation of GRASP65 by CDK1 and/or PLK1 [42,56,61,62]. Further Golgi breakdown into vesicular tubular clusters and the vesicular haze has been proposed to involve ongoing budding of COPI vesicles (**Figure 16**, step 5), whose tethering and fusion with Golgi membranes is blocked by CDK1- and PLK1-dependent phosphorylation of GM130 [54,56,61,63]. Alternatively, CDK1-mediated phosphorylation of Rab1A [42] and the ARF exchange factor GBF1 [33] at the pcIC membranes could block forward transport to the Golgi (**Figure 16**, step 2), while allowing the transfer of Golgi components to the IC. In this case, phosphorylation of GRASP65 and GM130 could instead inhibit vesicle tethering with the IC membranes, resulting in further dispersal of Golgi components via formation of IC-derived COPI vesicles (**Figure 16**, Step 4) [39,40,56]. Importantly, the localization of activated mitotic kinases close to the centrosomes at prophase [63] raises the possibility that the nearby pcIC membranes play an important role in the signaling pathways that initiate and monitor Golgi disassembly.

The alternative model of Golgi partitioning (**Figure 16**) is in accordance with previous studies demonstrating that Golgi enzymes display striking BFA-insensitivity (i.e., failure to redistribute to the ER) between prometaphase and late anaphase [72,76], thus indicating that they are temporarily present in the BFA-resistant mitotic IC elements at this particular stage. The present results (**Figure 13**) support this conclusion by showing that BFA treatment causes the accumulation of Man II in large Rab1A-positive membrane clusters, indicating that the IC acts as a way station during the redistribution of this enzyme to the Golgi haze. Importantly, the addition of BFA prior to mitosis redistributes Man II to the ER, and as a consequence, nearly all metaphasic cells display a diffuse Man II pattern ("haze"), verifying the time dependency of the drug effect (**Figure 13C**).

Notably, COPI coats maintain their association with the IC during mitosis, but can be effectively removed by BFA (**Figure 13B**). Thus, BFA most likely inhibits the dispersal of Man II into the

Golgi haze by blocking the formation of IC-derived COPI vesicles (**Figures 16** and **17B** below). Besides affecting the redistribution of Man II, the removal of COPI coats results in considerable enlargement of the mitotic IC clusters, indicating that the coats play an important role in determining the architecture of these structures [17,26].

Interestingly, treatment of mitotic cells with three different acidification inhibitors resulted in a similar block in Man II relocation as observed with BFA (**Figures 10A**, **11A**, and **11B**). Since the inhibitors have different mechanisms of action (see Section 1.4.4), these results are unlikely to be indirect, but rather highlight the importance of acidification for the mitotic redistribution of Golgi enzymes. Previous work with interphasic cells suggested that lumenal pH is important for COPI vesicle formation [49]. Notably, however, NH_4Cl treatment does not seem to affect the binding of COPI coats to the mitotic IC elements (data not shown), indicating that neutralization somehow affects COPI function without removing the coats, possibly by preventing their normal detachment or vesicle fusion. Thus, like BFA, acidification inhibitors may block the mitotic redistribution of Golgi components by inhibiting COPI-dependent pathways (**Figures 16** and **17B** below).

Surprisingly, quantification of the Man II distribution patterns in untreated metaphasic cells gave variable results in different experiments. While in the NH_4Cl experiment with parental NRK cells (**Figure 10B**), cells exhibiting the "punctate" pattern (45%) were outnumbered by those displaying the "haze" (55%), the BFA experiment (**Figure 13C**) instead indicated that the punctate pattern predominates (65%). This discrepancy could be explained by methodological differences, i.e., the fact that in the former experiment, metaphasic cells were analyzed *in situ* after fixation of steady state cultures, whereas in the latter experiment, the cells were synchronized (flush assay) and released by shake-off. Moreover, it is possible that the punctate pattern is typical for early metaphasic cells (**Figure 16**), whereas the haze pattern appears at a later stage, reflecting the relocation of Golgi enzymes from the "puncta" to dispersed vesicles. Accordingly, the synchronized cells appearing early after the flush could predominantly display the punctate pattern, corresponding to the initial accumulation of Golgi enzymes in the IC clusters (see Section 7). Importantly, the above considerations may account for the findings showing that the metaphasic Golgi of different cell types consists of variable amounts of large vesicular tubular clusters and small vesicles [54].

6.2 Trafficking functions of the IC during different stages of the cell cycle

Interestingly, although NH_4Cl completely blocks the redistribution of Man II during mitosis, it only partially affects its relocation to the ER in BFA-treated interphasic cells (**Figure 8A**). These differential effects may be reconciled with the help of a simplified model (**Figure 17**), proposing that the trafficking functions of the IC change through the course of the cell cycle. As depicted in the model, studies of interphasic cells have shown that the IC consists of two functionally distinct parts, a vacuolar domain containing ERGIC-53/p58 and COPI, and a tubular domain enriched in Rab1A, in accordance with the function of this compartment in vesicular (COPI-dependent) and tubular (COPI-independent) trafficking [7,9,28,31,64]. Furthermore, different types of COPI coats interacting with various SNAREs are likely to participate in the anterograde movement of cargo from the IC to the Golgi and in retrograde traffic to the ER [7,22,32,35-37]. Although the IC appears to maintain its division into COPI- and Rab1A-enriched subdomains during cell division (M. Marie, H. Dale, N. Kouprina, J. Saraste, manuscript in preparation; see **Figure 17B**), live-cell imaging has revealed that mitotic cells lack the dynamic Rab1A-containing tubules typical for interphasic cells. This inhibition of tubular trafficking could be due to CDK1-mediated phosphorylation of Rab1A [42,77], possibly affecting its interaction with a motor protein. By contrast, COPI coats still bind to the mitotic IC clusters (**Figure 13B**), indicating that COPI-dependent pathway(s) remain operational. As a consequence, acidification inhibitors, such as NH_4Cl, efficiently block Man II redistribution during mitosis by inhibiting COPI-dependent trafficking (**Figure 17B**), while BFA also gives a similar effect.

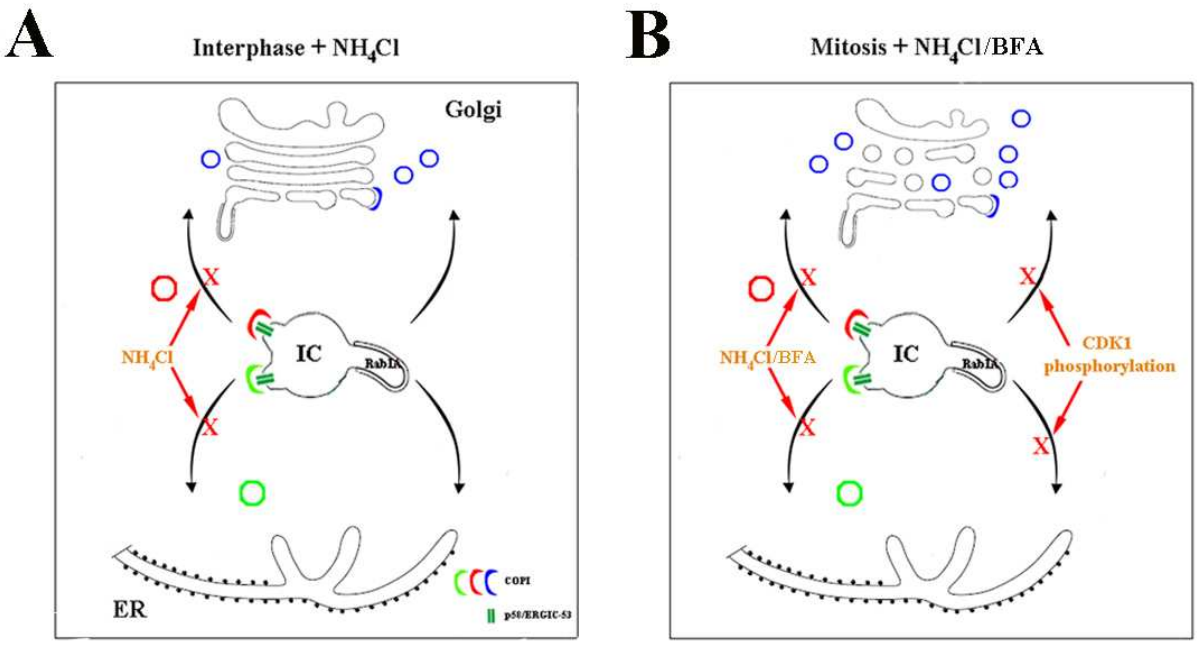

Figure 17. Cell cycle-dependent effects of NH_4Cl and BFA on the redistribution of Golgi components. (A) During interphase, the IC is the site of formation of two types of transport intermediates. Its vacuolar domain, which contains ERGIC-53/p58 and COPI, is involved in COPI-mediated vesicular trafficking. Anterograde transport to the Golgi and retrograde transport to the ER are mediated by two distinct types of COPI-coated vesicles (shown in red and green, respectively). The tubular IC domain containing the GTPase Rab1A is involved in COPI-independent tubular trafficking. For simplicity, only pathways originating at the IC are shown (COPII-mediated transport from the ER and COPI-mediated recycling pathways from the Golgi are not included). During interphase, NH_4Cl addition blocks the COPI-mediated pathways originating at the IC. However, COPI-independent, Rab1A-mediated tubular pathways remain functional and can redistribute Golgi enzymes to the ER after BFA addition. (B) The IC maintains its division into distinct vacuolar and tubular subdomains during mitosis. However, tubular trafficking is blocked due to CDK1-mediated phosphorylation of Rab1A. Furthermore, anterograde transport from the IC to the Golgi is blocked during mitosis, as previously suggested in **Figure 16** (not shown). Nevertheless, other COPI-mediated pathways are likely to remain functional, as indicated by the binding of COPI coats to the mitotic IC structures. The treatment of mitotic cells with NH_4Cl results in the accumulation of Golgi enzymes in the IC clusters by blocking their COPI-mediated redistribution into the mitotic haze. Similarly, BFA addition during mitosis blocks the dispersal of Golgi enzymes into the haze by affecting the function of the COPI coats. The model has been prepared by the author.

Treatment of interphasic cells with BFA results in the release of membrane-bound COPI coats, Golgi disassembly, and the transfer of Man II to the ER, which occurs (at least partly) via the pcIC [7]. As in mitosis, NH_4Cl may interfere with COPI-dependent trafficking from the IC, for example, by affecting the lumenal pH conditions required for the detachment of COPI vesicles [49].

However, the ongoing Rab1A-mediated tubular pathways allow Man II to reach the ER in the presence of the drug (**Figure 17A**). In fact, these tubular pathways may even be enhanced, not only by BFA [7,17,26,31], but possibly also by NH_4Cl, as shown by the increased tubulation of the pcIC observed after long-term treatment with acidification inhibitors (data not shown). Thus, in contrast to exerting a tight transport block during mitosis, NH_4Cl only partially arrests BFA-induced Man II redistribution during interphase. Notably, these results are consistent with previous studies on the effects of monensin and bafilomycin A1 on Man II redistribution following BFA treatment [7,49], suggesting that acidification of the IC lumen is required for retrograde trafficking.

One possibility is that the delay in Man II redistribution to the ER is due to an effect of NH_4Cl on the pcIC pool of Man II prior to BFA addition. Because this protein cycles between the Golgi and the pcIC during interphase [7], long-term (3 h) pretreatment with NH_4Cl and the resulting possible effects on COPI-mediated pathways may significantly increase this pool. However, quantification of the Man II signal in the pcIC did not show significant differences between control and NH_4Cl-treated cells (**Figure 9B**). Another alternative explanation for the observed delay is that the effect of BFA on COPI release is reduced due to the long-term NH_4Cl pretreatment, and therefore, some COPI-dependent pathways remain functional at early time points after BFA addition. Therefore, as during mitosis, NH_4Cl may block COPI-dependent pathways originating at the IC, resulting in temporary accumulation of Man II in the pcIC. The efficacy of BFA on COPI release after NH_4Cl pretreatment was not verified in these studies. NH_4Cl may also alter tubular trafficking during interphase, resulting in the observed delay in Man II redistribution. These alternatives need to be addressed by further experiments.

The effect of acidification inhibitors on the anterograde transport of CFTR, a chloride channel that uses an unconventional Golgi-independent pathway to reach the PM [78-80], was also examined. Previous studies showed that long-term BFA treatment results in CFTR relocation to the ER [78]; however, following BFA washout, the protein is transported to the cell surface via the pcIC [7]. Therefore, attempts were made to arrest CFTR trafficking by neutralizing the pcIC; however, the inhibitors did not seem to affect the transport of this protein to the PM after BFA washout (data not shown). Similarly, BFA washout in the presence of NH_4Cl did not affect the transfer of Man II from the ER to the Golgi (data not shown). This may indicate that acidification only plays a role in retrograde trafficking from the pcIC, possibly by affecting the formation of COPI vesicles

[49]. However, the above results were not quantified, and further experiments are required to determine the effect of neutralizing agents on anterograde trafficking. It would also be interesting to study the anterograde trafficking of other cargo proteins (e.g., VSV-G, SFV-G) in the presence of acidification inhibitors. This could provide better insight into the distinct mechanisms of anterograde and retrograde trafficking at the ER-Golgi boundary.

6.3 Effect of low temperature on membrane trafficking

As a final note, low temperature treatment of mitotic cells appeared to increase the accumulation of Man II in the Rab1A-positive IC clusters (see **Figures 14A-C**), indicating that it blocks the dispersal of Man II into the Golgi haze similar to BFA and the acidification inhibitors. A previous study concluded that low temperature incubation (15^{o}C) destabilizes microtubules and consequently disrupts the structure of the mitotic spindle [55]. Therefore, low temperature-induced disruption of spindle integrity may block the dispersal of Man II into the mitotic haze, leading to its accumulation in the IC clusters at metaphase. However, low temperature may also have an additional effect on membrane fluidity, blocking a specific step required for Golgi disassembly, such as membrane budding or fusion. It has also been reported that low temperature treatment during interphase affects COPI binding to membranes, thereby affecting vesicle budding [17,81,82]. A similar block in COPI budding during mitosis may lead to a block in Golgi disassembly, resulting in the observed pattern, i.e., Man II accumulation in large membrane clusters. Surprisingly, results from the subsequent quantification experiment show a completely opposite effect (see **Figure 14D**). These discrepant results may be due to the different preparation steps employed for the two experiments. While the low temperature effect was observed in mitotic cells that were first replated on coverslips prior to low temperature incubation, the quantification experiment was performed with shake-offs of mitotic cells treated with low temperature *in situ*. Because of these discrepancies, it is difficult to draw conclusions from these preliminary findings.

7 Conclusions and further perspectives

The results presented in this thesis provide evidence in support of an alternative model of mitotic Golgi partitioning, indicating that the permanent IC clusters function as way stations in the redistribution of Golgi enzymes. The similar effects of BFA and the acidification inhibitors suggest that the dispersal of the enzymes into the mitotic Golgi haze is mediated by COPI vesicles that bud from the IC elements. Accordingly, lumenal acidification of the IC is required for vesicle formation, or another aspect of COPI function. Both the proposed model of Golgi partitioning and the effect of pH disruption on coat assembly need to be addressed by additional experiments.

One possibility to validate the proposed mechanism of Golgi partitioning via the IC is to conduct the flush assay and follow in more detail Man II distribution under the synchronized conditions, i.e., at 5 min intervals after the flush. An initial predominance of the punctate pattern and gradual emergence of the haze would provide strong support for a model of Golgi partitioning involving the permanent IC clusters as way stations in the redistribution of Golgi components. In addition, it is necessary to repeat the experiment with NH_4Cl by employing the flush assay in the same manner as with BFA, rather than exposing cells to drug pretreatment. In the experiments with mitotic cells, the long-term pretreatments with acidification inhibitors were adopted based on results obtained with interphasic cells [49], as described earlier. However, the drugs may be more effective in mitotic cells, and therefore, long pretreatments may not be necessary. Furthermore, the addition of the drug at the time of the flush will diminish the possibility of secondary effects resulting from the long-term treatments. It will be interesting to see whether NH_4Cl addition immediately after flush causes rapid accumulation of Man II in the Rab1A-positive IC clusters at metaphase, as was observed with BFA. Finally, it will be important to repeat the cell fractionation experiments in order to verify Man II and Rab1 colocalization in mitotic cells by an alternative method. Electron microscopy should also be used to examine protein colocalization at the ultrastructural level. These proposed experiments would provide additional insight into the role of the IC in membrane trafficking during different stages of the cell cycle.

8 References

1 Mellman, I. & Warren, G. The road taken: past and future foundations of membrane traffic. *Cell* **100**, 99-112 (2000).

2 Bonifacino, J. S. & Glick, B. S. The mechanisms of vesicle budding and fusion. *Cell* **116**, 153-166 (2004).

3 Pelham, H. R. The Croonian Lecture 1999. Intracellular membrane traffic: getting proteins sorted. *Philos Trans R Soc Lond B Biol Sci* **354**, 1471-1478, doi:10.1098/rstb.1999.0491 (1999).

4 Storrie, B. & Nilsson, T. The Golgi apparatus: balancing new with old. *Traffic* **3**, 521-529 (2002).

5 Nakamura, N. Emerging new roles of GM130, a cis-Golgi matrix protein, in higher order cell functions. *J Pharmacol Sci* **112**, 255-264 (2010).

6 Alberts, B. Molecular Biology of the Cell. (Garland Science, Taylor & Francis group, 2008).

7 Marie, M., Dale, H. A., Sannerud, R. & Saraste, J. The function of the intermediate compartment in pre-Golgi trafficking involves its stable connection with the centrosome. *Mol Biol Cell* **20**, 4458-4470, doi:10.1091/mbc.E08-12-1229 (2009).

8 Grant, B. D. & Donaldson, J. G. Pathways and mechanisms of endocytic recycling. *Nat Rev Mol Cell Biol* **10**, 597-608, doi:10.1038/nrm2755 (2009).

9 Saraste, J. & Goud, B. Functional symmetry of endomembranes. *Mol Biol Cell* **18**, 1430-1436, doi:10.1091/mbc.E06-10-0933 (2007).

10 Sannerud, R., Saraste, J. & Goud, B. Retrograde traffic in the biosynthetic-secretory route: pathways and machinery. *Curr Opin Cell Biol* **15**, 438-445 (2003).

11 Bannykh, S. I., Nishimura, N. & Balch, W. E. Getting into the Golgi. *Trends Cell Biol* **8**, 21-25 (1998).

12 Hauri, H. P., Kappeler, F., Andersson, H. & Appenzeller, C. ERGIC-53 and traffic in the secretory pathway. *J Cell Sci* **113 (Pt 4)**, 587-596 (2000).

13 Nickel, W., Brugger, B. & Wieland, F. T. Protein and lipid sorting between the endoplasmic reticulum and the Golgi complex. *Semin Cell Dev Biol* **9**, 493-501, doi:10.1006/scdb.1998.0256 (1998).

14 Klumperman, J. Transport between ER and Golgi. *Curr Opin Cell Biol* **12**, 445-449 (2000).

15 Xu, D. & Hay, J. C. Reconstitution of COPII vesicle fusion to generate a pre-Golgi intermediate compartment. *J Cell Biol* **167**, 997-1003, doi:10.1083/jcb.200408135 (2004).

16 Saraste, J. & Kuismanen, E. Pathways of protein sorting and membrane traffic between the rough endoplasmic reticulum and the Golgi complex. *Semin Cell Biol* **3**, 343-355 (1992).

17 Tomas, M., Martinez-Alonso, E., Ballesta, J. & Martinez-Menarguez, J. A. Regulation of ER-Golgi intermediate compartment tubulation and mobility by COPI coats, motor proteins and microtubules. *Traffic* **11**, 616-625, doi:10.1111/j.1600-0854.2010.01047.x (2010).

18 Appenzeller-Herzog, C. & Hauri, H. P. The ER-Golgi intermediate compartment (ERGIC): in search of its identity and function. *J Cell Sci* **119**, 2173-2183, doi:10.1242/jcs.03019 (2006).

19 Ben-Tekaya, H., Miura, K., Pepperkok, R. & Hauri, H. P. Live imaging of bidirectional traffic from the ERGIC. *J Cell Sci* **118**, 357-367, doi:10.1242/jcs.01615 (2005).

20 Martinez-Menarguez, J. A. *et al.* Peri-Golgi vesicles contain retrograde but not anterograde proteins consistent with the cisternal progression model of intra-Golgi transport. *J Cell Biol* **155**, 1213-1224, doi:10.1083/jcb.200108029 (2001).

21 Glick, B. S. & Nakano, A. Membrane traffic within the Golgi apparatus. *Annu Rev Cell Dev Biol* **25**, 113-132, doi:10.1146/annurev.cellbio.24.110707.175421 (2009).

22 Emr, S. *et al.* Journeys through the Golgi--taking stock in a new era. *J Cell Biol* **187**, 449-453, doi:10.1083/jcb.200909011 (2009).

23 Orci, L., Amherdt, M., Ravazzola, M., Perrelet, A. & Rothman, J. E. Exclusion of golgi residents from transport vesicles budding from Golgi cisternae in intact cells. *J Cell Biol* **150**, 1263-1270 (2000).

24 Prydz, K., Dick, G. & Tveit, H. How many ways through the Golgi maze? *Traffic* **9**, 299-304, doi:10.1111/j.1600-0854.2007.00690.x (2008).

25 Marie, M., Sannerud, R., Avsnes Dale, H. & Saraste, J. Take the 'A' train: on fast tracks to the cell surface. *Cell Mol Life Sci* **65**, 2859-2874, doi:10.1007/s00018-008-8355-0 (2008).

26 Klausner, R. D., Donaldson, J. G. & Lippincott-Schwartz, J. Brefeldin A: insights into the control of membrane traffic and organelle structure. *J Cell Biol* **116**, 1071-1080 (1992).

27 Ward, T. H., Polishchuk, R. S., Caplan, S., Hirschberg, K. & Lippincott-Schwartz, J. Maintenance of Golgi structure and function depends on the integrity of ER export. *J Cell Biol* **155**, 557-570, doi:10.1083/jcb.200107045 (2001).

28 Sannerud, R. *et al.* Rab1 defines a novel pathway connecting the pre-Golgi intermediate compartment with the cell periphery. *Mol Biol Cell* **17**, 1514-1526, doi:10.1091/mbc.E05-08-0792 (2006).

29 Saraste, J., Lahtinen, U. & Goud, B. Localization of the small GTP-binding protein rab1p to early

compartments of the secretory pathway. *J Cell Sci* **108 (Pt 4)**, 1541-1552 (1995).

30 Juschke, C., Wachter, A., Schwappach, B. & Seedorf, M. SEC18/NSF-independent, protein-sorting pathway from the yeast cortical ER to the plasma membrane. *J Cell Biol* **169**, 613-622, doi:10.1083/jcb.200503033 (2005).

31 Saraste, J., Dale, H. A., Bazzocco, S. & Marie, M. Emerging new roles of the pre-Golgi intermediate compartment in biosynthetic-secretory trafficking. *FEBS Lett* **583**, 3804-3810, doi:10.1016/j.febslet.2009.10.084 (2009).

32 Beck, R., Rawet, M., Wieland, F. T. & Cassel, D. The COPI system: molecular mechanisms and function. *FEBS Lett* **583**, 2701-2709, doi:10.1016/j.febslet.2009.07.032 (2009).

33 Morohashi, Y., Balklava, Z., Ball, M., Hughes, H. & Lowe, M. Phosphorylation and membrane dissociation of the ARF exchange factor GBF1 in mitosis. *Biochem J* **427**, 401-412, doi:10.1042/BJ20091681 (2010).

34 Zhao, X., Lasell, T. K. & Melancon, P. Localization of large ADP-ribosylation factor-guanine nucleotide exchange factors to different Golgi compartments: evidence for distinct functions in protein traffic. *Mol Biol Cell* **13**, 119-133, doi:10.1091/mbc.01-08-0420 (2002).

35 Moelleken, J. *et al.* Differential localization of coatomer complex isoforms within the Golgi apparatus. *Proc Natl Acad Sci U S A* **104**, 4425-4430, doi:10.1073/pnas.0611360104 (2007).

36 Futatsumori, M., Kasai, K., Takatsu, H., Shin, H. W. & Nakayama, K. Identification and characterization of novel isoforms of COP I subunits. *J Biochem* **128**, 793-801 (2000).

37 Sahlmuller, M. C. *et al.* Recombinant Heptameric Coatomer Complexes: Novel Tools to Study Isoform-Specific Functions. *Traffic* **12**, 682-692, doi:10.1111/j.1600-0854.2011.01177.x (2011).

38 Stenmark, H. Rab GTPases as coordinators of vesicle traffic. *Nat Rev Mol Cell Biol* **10**, 513-525, doi:10.1038/nrm2728 (2009).

39 Short, B., Haas, A. & Barr, F. A. Golgins and GTPases, giving identity and structure to the Golgi apparatus. *Biochim Biophys Acta* **1744**, 383-395, doi:10.1016/j.bbamcr.2005.02.001 (2005).

40 Wei, J. H. & Seemann, J. Mitotic division of the mammalian Golgi apparatus. *Semin Cell Dev Biol* **20**, 810-816, doi:10.1016/j.semcdb.2009.03.010 (2009).

41 Diao, A., Frost, L., Morohashi, Y. & Lowe, M. Coordination of golgin tethering and SNARE assembly: GM130 binds syntaxin 5 in a p115-regulated manner. *J Biol Chem* **283**, 6957-6967, doi:10.1074/jbc.M708401200 (2008).

42 Preisinger, C. *et al.* Plk1 docking to GRASP65 phosphorylated by Cdk1 suggests a mechanism for Golgi checkpoint signalling. *Embo J* **24**, 753-765, doi:10.1038/sj.emboj.7600569 (2005).

43 Puthenveedu, M. A. & Linstedt, A. D. Evidence that Golgi structure depends on a p115 activity that is independent of the vesicle tether components giantin and GM130. *J Cell Biol* **155**, 227-238, doi:10.1083/jcb.200105005 (2001).

44 Weisz, O. A. Organelle acidification and disease. *Traffic* **4**, 57-64 (2003).

45 Weisz, O. A. Acidification and protein traffic. *Int Rev Cytol* **226**, 259-319 (2003).

46 Paroutis, P., Touret, N. & Grinstein, S. The pH of the secretory pathway: measurement, determinants, and regulation. *Physiology (Bethesda)* **19**, 207-215, doi:10.1152/physiol.00005.2004 (2004).

47 Axelsson, M. A. *et al.* Neutralization of pH in the Golgi apparatus causes redistribution of glycosyltransferases and changes in the O-glycosylation of mucins. *Glycobiology* **11**, 633-644 (2001).

48 Rivinoja, A., Hassinen, A., Kokkonen, N., Kauppila, A. & Kellokumpu, S. Elevated Golgi pH impairs terminal N-glycosylation by inducing mislocalization of Golgi glycosyltransferases. *J Cell Physiol* **220**, 144-154, doi:10.1002/jcp.21744 (2009).

49 Palokangas, H., Ying, M., Vaananen, K. & Saraste, J. Retrograde transport from the pre-Golgi intermediate compartment and the Golgi complex is affected by the vacuolar H+-ATPase inhibitor bafilomycin A1. *Mol Biol Cell* **9**, 3561-3578 (1998).

50 Ying, M., Flatmark, T. & Saraste, J. The p58-positive pre-golgi intermediates consist of distinct subpopulations of particles that show differential binding of COPI and COPII coats and contain vacuolar H(+)-ATPase. *J Cell Sci* **113 (Pt 20)**, 3623-3638 (2000).

51 Scheel, A. A. & Pelham, H. R. Purification and characterization of the human KDEL receptor. *Biochemistry* **35**, 10203-10209, doi:10.1021/bi960807x (1996).

52 Appenzeller-Herzog, C., Roche, A. C., Nufer, O. & Hauri, H. P. pH-induced conversion of the transport lectin ERGIC-53 triggers glycoprotein release. *J Biol Chem* **279**, 12943-12950, doi:10.1074/jbc.M313245200 (2004).

53 Ying, M., Sannerud, R., Flatmark, T. & Saraste, J. Colocalization of Ca2+-ATPase and GRP94 with p58 and the effects of thapsigargin on protein recycling suggest the participation of the pre-Golgi intermediate compartment in intracellular Ca2+ storage. *Eur J Cell Biol* **81**, 469-483 (2002).

54 Puthenveedu, M. A. & Linstedt, A. D. In search of an essential step during mitotic Golgi disassembly and inheritance. *Exp Cell Res* **271**, 22-27, doi:10.1006/excr.2001.5367 (2001).

55 Jesch, S. A., Mehta, A. J., Velliste, M., Murphy, R. F. & Linstedt, A. D. Mitotic Golgi is in a dynamic equilibrium between clustered and free vesicles independent of the ER. *Traffic* **2**, 873-884 (2001).

56 Wei, J. H. & Seemann, J. Unraveling the Golgi ribbon. *Traffic* **11**, 1391-1400, doi:10.1111/j.1600-0854.2010.01114.x (2010).

57 Farmaki, T. *et al.* Forward and retrograde trafficking in mitotic animal cells. ER-Golgi transport arrest restricts protein export from the ER into COPII-coated structures. *J Cell Sci* **112 (Pt 5)**, 589-600 (1999).

58 Colanzi, A., Suetterlin, C. & Malhotra, V. Cell-cycle-specific Golgi fragmentation: how and why? *Curr Opin Cell Biol* **15**, 462-467 (2003).

59 Zaal, K. J. *et al.* Golgi membranes are absorbed into and reemerge from the ER during mitosis. *Cell* **99**, 589-601 (1999).

60 Gaietta, G. M. *et al.* Golgi twins in late mitosis revealed by genetically encoded tags for live cell imaging and correlated electron microscopy. *Proc Natl Acad Sci U S A* **103**, 17777-17782, doi:10.1073/pnas.0608509103 (2006).

61 Sutterlin, C. *et al.* Polo-like kinase is required for the fragmentation of pericentriolar Golgi stacks during mitosis. *Proc Natl Acad Sci U S A* **98**, 9128-9132, doi:10.1073/pnas.161283998 (2001).

62 Vinke, F. P., Grieve, A. G. & Rabouille, C. The multiple facets of the Golgi reassembly stacking proteins. *Biochem J* **433**, 423-433, doi:10.1042/BJ20101540 (2011).

63 Sutterlin, C. & Colanzi, A. The Golgi and the centrosome: building a functional partnership. *J Cell Biol* **188**, 621-628, doi:10.1083/jcb.200910001 (2010).

64 Pavelka, M., Neumuller, J. & Ellinger, A. Retrograde traffic in the biosynthetic-secretory route. *Histochem Cell Biol* **129**, 277-288, doi:10.1007/s00418-008-0383-1 (2008).

65 Seemann, J., Pypaert, M., Taguchi, T., Malsam, J. & Warren, G. Partitioning of the matrix fraction of the Golgi apparatus during mitosis in animal cells. *Science* **295**, 848-851, doi:10.1126/science.1068064 (2002).

66 Wei, J. H. & Seemann, J. The mitotic spindle mediates inheritance of the Golgi ribbon structure. *J Cell Biol* **184**, 391-397, doi:10.1083/jcb.200809090 (2009).

67 Seemann, J., Jokitalo, E., Pypaert, M. & Warren, G. Matrix proteins can generate the higher order architecture of the Golgi apparatus. *Nature* **407**, 1022-1026, doi:10.1038/35039538 (2000).

68 McKay, H. F. & Burgess, D. R. 'Life is a highway': membrane trafficking during cytokinesis. *Traffic* **12**, 247-251, doi:10.1111/j.1600-0854.2010.01139.x (2011).

69 Sharma, M. *et al.* Misfolding diverts CFTR from recycling to degradation: quality control at early endosomes. *J Cell Biol* **164**, 923-933, doi:10.1083/jcb.200312018 (2004).

70 Saraste, J. & Svensson, K. Distribution of the intermediate elements operating in ER to Golgi transport. *J Cell Sci* **100 (Pt 3)**, 415-430 (1991).

71 Sannerud, R., Marie, M., Hansen, B. B. & Saraste, J. Use of polarized PC12 cells to monitor protein localization in the early biosynthetic pathway. *Methods Mol Biol* **457**, 253-265 (2008).

72 Nizak, C. *et al.* Golgi inheritance under a block of anterograde and retrograde traffic. *Traffic* **5**, 284-299, doi:10.1111/j.1398-9219.2004.0174.x (2004).

73 Kramer, A., Lukas, J. & Bartek, J. Checking out the centrosome. *Cell Cycle* **3**, 1390-1393 (2004).

74 Jackman, M., Lindon, C., Nigg, E. A. & Pines, J. Active cyclin B1-Cdk1 first appears on centrosomes in prophase. *Nat Cell Biol* **5**, 143-148, doi:10.1038/ncb918 (2003).

75 Rios, R. M. & Bornens, M. The Golgi apparatus at the cell centre. *Curr Opin Cell Biol* **15**, 60-66 (2003).

76 Jesch, S. A. & Linstedt, A. D. The Golgi and endoplasmic reticulum remain independent during mitosis in HeLa cells. *Mol Biol Cell* **9**, 623-635 (1998).

77 Dephoure, N. *et al.* A quantitative atlas of mitotic phosphorylation. *Proc Natl Acad Sci U S A* **105**, 10762-10767, doi:10.1073/pnas.0805139105 (2008).

78 Okiyoneda, T. *et al.* Characterization of the trafficking pathway of cystic fibrosis transmembrane conductance regulator in baby hamster kidney cells. *J Pharmacol Sci* **95**, 471-475 (2004).

79 Yoo, J. S. *et al.* Non-conventional trafficking of the cystic fibrosis transmembrane conductance regulator through the early secretory pathway. *J Biol Chem* **277**, 11401-11409, doi:10.1074/jbc.M110263200 (2002).

80 Bannykh, S. I. *et al.* Traffic pattern of cystic fibrosis transmembrane regulator through the early exocytic pathway. *Traffic* **1**, 852-870 (2000).

81 Martinez-Alonso, E., Egea, G., Ballesta, J. & Martinez-Menarguez, J. A. Structure and dynamics of the Golgi complex at 15 degrees C: low temperature induces the formation of Golgi-derived tubules. *Traffic* **6**, 32-44, doi:10.1111/j.1600-0854.2004.00242.x (2005).

82 Martinez-Alonso, E., Tomas, M., Ballesta, J. & Martinez-Menarguez, J. A. Low temperature (15 degrees C) induces COPII dissociation from membranes and slow exit from the endoplasmic reticulum in HeLa cells. *Histochem Cell Biol* **128**, 379-384, doi:10.1007/s00418-007-0317-3 (2007).